NASA TECHNICAL REPORT

NASA TR R-203

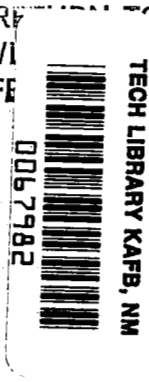

THEORY OF TUMBLING BODIES ENTERING PLANETARY ATMOSPHERES WITH APPLICATION TO PROBE VEHICLES AND THE AUSTRALIAN TEKTITES

by Murray Tobak and Victor L. Peterson

Ames Research Center
Moffett Field, Calif.

NATIONAL AERONAUTICS AND SPACE ADMINISTRATION • WASHINGTON, D. C. • JULY 1964

THEORY OF TUMBLING BODIES ENTERING PLANETARY ATMOSPHERES WITH APPLICATION TO PROBE VEHICLES AND THE AUSTRALIAN TEKTITES

By Murray Tobak and Victor L. Peterson

Ames Research Center
Moffett Field, Calif.

NATIONAL AERONAUTICS AND SPACE ADMINISTRATION

For sale by the Office of Technical Services, Department of Commerce,
Washington, D.C. 20230 -- Price $1.00

THEORY OF TUMBLING BODIES ENTERING PLANETARY ATMOSPHERES WITH APPLICATION TO PROBE VEHICLES AND THE AUSTRALIAN TEKTITES

By Murray Tobak and Victor L. Peterson

Ames Research Center
Moffett Field, Calif.

SUMMARY

The tumbling motion of aerodynamically stable bodies entering planetary atmospheres is analyzed considering that the tumbling, its arrest, and the subsequent oscillatory motion are governed by the equation for the fifth Painlevé transcendent. Results based on the asymptotic behavior of the transcendent are applied to study (1) the oscillatory behavior of planetary probe vehicles in relation to aerodynamic heating and loads and (2) the dynamic behavior of the Australian tektites on entering the Earth's atmosphere, under the hypothesis that their origin was the Moon.

INTRODUCTION

When a body in space is separated from a parent body, in most cases the separation process will leave the body with a measure of angular momentum. The body then will tumble at a constant rate about its center of gravity for the remainder of its sojourn in space. As it enters a planetary atmosphere, however, its tumbling rate will begin to be affected by the aerodynamic forces and moments that come into play as the dynamic pressure builds up. If the body's shape is such as to provide a measure of aerodynamic stability, the increasing aerodynamic moment eventually will bring the tumbling rate to zero. Subsequently, the body will undergo an oscillatory motion of possibly large but diminishing amplitude. It is of interest to analyze the sequence both in connection with the design of vehicles destined to make uncontrolled entries into planetary atmospheres and in connection with the study of the motions of extraterrestrial objects that have found their way into the Earth's atmosphere.

The equations governing a tumbling entry are inherently nonlinear and hence difficult to treat analytically. The first investigation in this field therefore was a numerical study (ref. 1) of a particular vehicle entering a specific atmosphere (Mars'). Subsequently, an analytical treatment of the problem was reported in reference 2. Results of that study showed that simplifying approximations could be made, enabling the tumbling motion, its arrest, and the subsequent oscillatory motion to be governed by a single differential equation. This equation was identified as the equation for the fifth Painlevé transcendent. Following that study, another analysis was

carried out (ref. 3) in which the functional relationships existing between the motion of the vehicle and the vehicle and planetary properties were deduced from the asymptotic behavior of the transcendent.

The purpose of the present work is to combine the analyses of references 2 and 3 in a unified treatment and to apply the results to two different types of problems. In the first, the tumbling entry of a probe vehicle is considered, and it is shown how the results may be used to make rapid estimates of the amplitudes of the oscillatory motion in relation to aerodynamic heating and loads. In the second, attention is directed to an aspect of the research on the origin of tektites. On the basis of the work of Chapman and Larson (ref. 4) the Australian tektites are taken to be of lunar origin and the consequent dynamic behavior of the tektites on entering the Earth's atmosphere is examined within the context of the present analysis.

SYMBOLS

A	reference area
B	parameter defined by equation (43)
C	parameter defined by equations (27)
C_D	drag coefficient, $\frac{\text{drag}}{qA}$
C_L	lift coefficient, $\frac{\text{lift}}{qA}$
C_m	pitching-moment coefficient, $\frac{\text{pitching moment}}{qA\ell}$
f	dependent variable, $\tan \epsilon$
g	acceleration due to gravity
G	parameter defined by equations (27)
H_s	stagnation-point heat transferred per unit area
I	pitching moment of inertia about center of gravity
I_z	moment of inertia about axis of spin
$J_0(x)$	Bessel function of first kind of zero order
$J_1(x)$	Bessel function of first kind of first order
ℓ	reference length for moment coefficient evaluation
m	body mass

n	integer, denoting number of complete tumbles
q	dynamic pressure, $\frac{1}{2}\rho V^2$
r	distance from center of planet to body
s	dynamic-pressure parameter, $\beta V_i \sin \gamma_i$
t	time
u	horizontal component of flight velocity (sketch (a))
v	vertical component of flight velocity (sketch (a))
V	flight velocity (sketch (a))
x	independent variable (eqs. (10))
X,Z	axes fixed in space with origin at planet center (sketch (a))
y	altitude
$Y_o(x)$	Bessel function of second kind of zero order
$Y_1(x)$	Bessel function of second kind of first order
$\bar{Z}_o(x)$	$\bar{a}J_o(x) + \bar{b}Y_o(x)$
α	angle of attack in planar motion (sketch (a))
β	density parameter (eq. (7))
γ	flight-path angle, positive when depressed from local horizontal (sketch (a))
ϵ	dependent variable (eq. (16))
ϵ_c	initial value of ϵ which causes body eventually to trim in backward attitude
$\Delta\epsilon_i$	increment in initial value of ϵ measured from ϵ_c (eq. (19))
Θ	angle of pitch measured from axis fixed in space (sketch (a))
θ	angle of pitch measured from local horizontal (sketch (a))
κ	initial value of x (eqs. (10)), $\sqrt{-\frac{4}{s^2} q_i \frac{Al}{I} C_{m_{max}}}$
λ	ablation parameter (eq. (63))
ρ	atmospheric density

ρ_o atmospheric density at surface of planet

σ resultant angle of attack in nonplanar motion (sketch (h))

ϕ angular displacement of body from fixed space axis, $\theta - \Theta$ (sketch(a))

ω angular velocity of rotating liquid (sketch (e))

$(\dot{})$ $\frac{d}{dt}(\ )$

$(\ )'$ $\frac{d}{dx}(\ )$

$(\ )_i$ initial value

$(\ )_p$ value of quantity at first peak of oscillatory motion

$(\ )_{max}$ maximum value of quantity

$(\ )_{min}$ minimum value of quantity

$(\ )_{env}$ envelope of oscillatory function

$(\ )_{mh}$ quantity evaluated at maximum heating

ANALYSIS

The analysis leading to a differential equation that can be said to characterize the tumbling entry problem was initially presented in reference 2. That analysis will be given here again in a slightly amended form to bring out its relevance to the study of the motions of extraterrestrial bodies as well as of vehicles. As before, in order to reduce the problem to manageable proportions, it is assumed at the outset that (1) the rotation of the planet and of its atmosphere may be neglected; (2) the motion is planar; and (3) the acceleration due to gravity is constant. Further assumptions and approximations will be introduced as necessary.

Equations of Motion

Under the above assumptions, the equations governing the body's path and its motions about that path may be written as

$$\left.\begin{aligned} -m\dot{V} - C_D qA + mg \sin\gamma &= 0 \\ mV\dot{\gamma} + C_L qA + m[(V^2/r) - g]\cos\gamma &= 0 \\ I\ddot{\Theta} - qAlC_m &= 0 \end{aligned}\right\} \qquad (1)$$

The angles α, γ, θ, ϕ, Θ are defined in sketch (a).

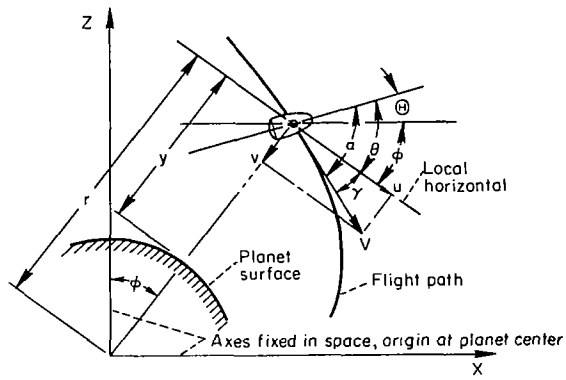

Sketch (a)

Simplified angle-of-attack equation.- Numerical solutions of equations (1) indicate that after the body enters the planetary atmosphere, there is always an interval over which the flight-path angle γ and the flight speed V do not change significantly. Since this is the interval over which any tumbling motion would occur, it is an appropriate approximation to take

$$\left.\begin{aligned} \gamma &\approx \text{const} = \gamma_i \\ V &\approx \text{const} = V_i \end{aligned}\right\} \qquad (2)$$

Then, since $\dot{\phi} = u/r$, $\ddot{\phi}$ will be essentially zero, so that

$$\ddot{\Theta} \approx \ddot{\alpha} \qquad (3)$$

Next, it will be assumed that aerodynamic damping-moment terms are negligible over the range of interest, so that the aerodynamic moment in equations (1) is a function of angle of attack only. This, in conjunction with equation (3), enables one to consider the last of equations (1) independently of the other two. That equation becomes

$$\ddot{\alpha} - \frac{Al}{I} q(t) C_m(\alpha) = 0 \qquad (4)$$

Aerodynamic restoring-moment coefficient.- As a body tumbles, it sweeps through the entire angle-of-attack range. The aerodynamic restoring-moment coefficient therefore must be specified over that entire range. Consider first a vehicle intended to act as a planetary probe. It is reasonable to anticipate that heating and stability considerations will dictate the choice of its shape, hence, that it will be short with a conic profile. Also, in order to minimize the amount of heat protection required, it is advisable that the vehicle be statically stable in one trim position only. In reference 1 it was found that the latter requirement could be fulfilled by the addition of a convex afterbody to the original conic forebody. Inspection of the experimental results collected in reference 1 for a vehicle of this shape reveals that the aerodynamic restoring-moment coefficient as a function of angle of attack is approximately a sine wave. Accordingly, it will be assumed that for the probe vehicle, $C_m(\alpha)$ in equation (4) may be approximated by

$$C_m(\alpha) = C_{m_{max}} \sin \alpha \qquad (5)$$

where $C_{m_{max}}$ is presumed to be available either from experimental data or, for example, from Newtonian impact theory. The choice of equation (5) as an appropriate form for the aerodynamic restoring-moment coefficient may be arrived at from another point of view. With the addition of a convex afterbody, the shape whose aerodynamic restoring-moment coefficient is reasonably

well approximated by equation (5) may, with a little imagination, be thought of as a modification to a sphere. Now it is easy to see that a sphere with its center of gravity displaced from its center of volume has, without approximation, precisely equation (5) as the form of its aerodynamic restoring-moment coefficient. In this light, therefore, it is not surprising that equation (5) should appear as the appropriate choice. In this light also, consider the tektites found in southeast Australia. As pointed out in reference 4, the primary shapes of about 80 percent of them, that is, their shapes on entering the atmosphere, were undoubtedly spheres or spheroids. The aerodynamic restoring-moment coefficient for a perfect sphere is, of course, identically zero; but with a small amount of oblateness which may be considered as an equivalent displacement of the mass center from the center of volume of a perfect sphere, the tektites then would have had aerodynamic restoring-moment coefficients of the form of equation (5). It is this fact that places the study of their motions within the framework of the present analysis.

Dynamic-pressure history.- Consistent with the approximations underlying equations (2), the altitude history of the body as a function of time is

$$y - y_i = -v_i t \tag{6}$$

where

$$v_i = V_i \sin \gamma_i$$

The assumption that the planet's atmospheric density varies exponentially with altitude

$$\rho = \rho_o e^{-\beta y} \tag{7}$$

then gives for the dynamic pressure over the range of interest

$$q(t) = q_i e^{\beta v_i t} \tag{8}$$

with

$$q_i = \frac{1}{2} \rho_o V_i^2 e^{-\beta y_i}$$

Alternatively, if a precise time history of the dynamic pressure is available, a more accurate estimate of q_i and βv_i may be obtained by fitting the best straight line to the initial portion of the dynamic-pressure history plotted on semilogarithmic paper. In this regard, it should be clear that equation (8) reveals one of the apparently more severe limitations of the present analysis, namely, that it can be expected to apply only over the portion of the time history in which $q(t)$ increases monotonically. However, it will be found that this interval encompasses not only the interval over which tumbling occurs, but also the subsequent range over which the oscillatory motion begins and is reduced to small angles. The results of this analysis should be suited to act as the connecting link between the body's initial behavior and the behavior described by the results of analyses in which the linear

approximation to the aerodynamic restoring moment has been introduced (ref. 5, e.g., which is applicable after the oscillatory motion has been reduced to small angles).

Transformed equation.- Inserting equations (5) and (8) into equation (4) gives

$$\ddot{\alpha} - q_i \frac{Al}{I} C_{m_{max}} e^{\beta v_i t} \sin \alpha = 0 \tag{9}$$

which will be taken to be the differential equation characterizing the tumbling entry problem. However, a transformation of equation (9) yields a form that more quickly shows the nature of the solution. Let

$$\left.\begin{aligned} \beta v_i &= s \\ -q_i \frac{Al}{I} C_{m_{max}} &= \left(\frac{\kappa s}{2}\right)^2 \\ \frac{x}{\kappa} &= e^{st/2} \end{aligned}\right\} \tag{10}$$

Equation (9) takes the form

$$\alpha''(x) + \frac{\alpha'(x)}{x} + \sin \alpha = 0 \tag{11}$$

with the initial conditions

$$\left.\begin{aligned} \alpha(\kappa) &= \alpha_i \\ \alpha'(\kappa) &= \frac{2}{\kappa s} \dot{\alpha}_i \end{aligned}\right\} \tag{12}$$

where, for convenience, $\alpha(\kappa)$ is presumed to lie within the range $-\pi \leq \alpha(\kappa) \leq \pi$. Note that all the parameters of the problem have been concentrated in the constant κ and the initial conditions. Equations (11) and (12) indicate that all combinations of body and planetary properties yielding the same value of κ and the same initial conditions $\alpha(\kappa)$, $\alpha'(\kappa)$ will yield identical solutions for α as a function of x, though not necessarily as a function of time. The independent variable x may be given a physical meaning when it is noted that, within the approximations made, it is proportional to the square root of the dynamic pressure q.

The Painlevé Transcendents

The substitution $w = \sin \alpha/2$ in equation (11) transforms it to

$$w''(x) = L(w)p^2 + M(x)p + N(w) \tag{13}$$

where

$$p = \frac{dw}{dx}$$

$$L(w) = \frac{w}{w^2 - 1}$$

$$M(x) = -\frac{1}{x}$$

$$N(w) = w(w^2 - 1)$$

In reference 6, it will be found that equation (13) is of the form studied by the French mathematician Paul Painlevé around 1900. It is categorized mathematically as being a member of the general class of second-order differential equations whose solutions have fixed critical points (i.e., no movable branch points or essential singularities). This class has been shown to possess 50 members. Of the 50, all but 6 are integrable in terms of known functions. The remaining 6 define new functions, termed "Painlevé transcendents." The substitution $W = (w + 1)/(w - 1)$ casts equation (13) in the form

$$W''(x) = W'^2 \left(\frac{1}{2W} + \frac{1}{W - 1}\right) - \frac{W'}{x} - 2W\left(\frac{W + 1}{W - 1}\right) \qquad (14)$$

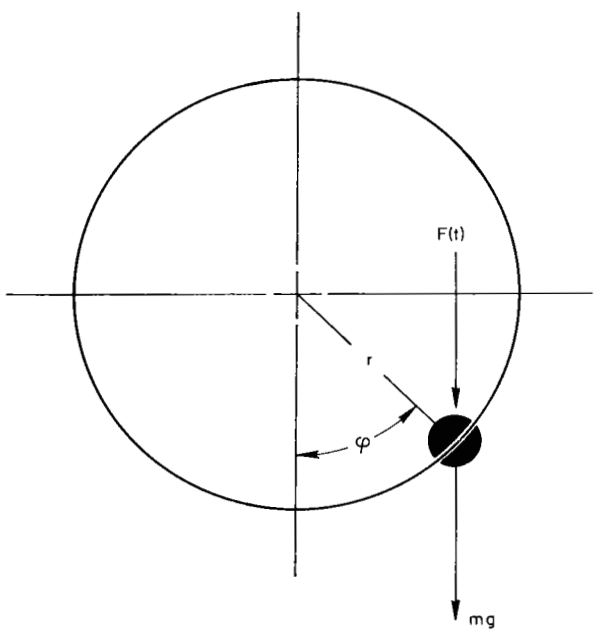

Sketch (b)

and it will be seen in reference 6 that equation (14) is one of these, namely, the fifth (with, in Ince's notation, $\alpha = \beta = \gamma = 0$, $\delta = -2$). Unfortunately, aside from this categorization and a comprehensive examination of the asymptotic behavior of the first Painlevé transcendent (ref. 7), no subsequent analyses of their properties seem to have been published.

Mechanical Analogy

Before proceeding, let us first consider a simple mechanical analogy of equation (9) whose behavior is, in effect, intuitively obvious. By this means, the range and character of motion governed by the equation can be revealed relatively simply.

Consider a small bead constrained to slide, without friction, on a circular path in a vertical plane. Let a time-dependent force F(t) be exerted downward on the bead. This situation is illustrated in sketch (b). Equating

the torque about the center of the circle to the bead's rate of change of angular momentum gives

$$\ddot{\varphi} + \frac{1}{r}\left[g + \frac{F(t)}{m}\right] \sin \varphi = 0 \qquad (15)$$

Thus, if $g + [F(t)/m]$ is caused to vary in proportion to the body's dynamic pressure history, the motion $\varphi(t)$ governed by equation (15) will be analogous to that of the body with φ playing the role of α.

For convenience, let $\varphi = 0$ (the bottom of the circle) at $t = 0$. Now give the bead an initial velocity sufficient to carry it several times around the circle. Each time the bead traverses the circle, φ will be counted as having increased by 2π. This, of course, corresponds to one complete tumble of the body. It is clear that, because $F(t)$ increases continually, more and more of the total energy will be in the form of potential energy each time the bead nears the top of the circle. Eventually, therefore, the bead will not have sufficient kinetic energy to carry it over the top. At this point, it will reverse direction, slide down past the low point, and proceed to oscillate about the low point. Again, because the amplitude of the restoring torque grows indefinitely with time, the amplitude of oscillation will diminish and the frequency will increase with time. The final value of φ will be a multiple of 2π. This behavior is illustrated as curve A in sketch (c) for a case where the bead has tumbled twice. Note in the sketch that once tumbling is arrested, the bead's amplitude of oscillation about $2n\pi$ cannot exceed π.[1] For a range of successively smaller initial velocities, the behavior of $\varphi(t)$ will be qualitatively similar to that just described, the tumbling in each case being arrested when φ is between $(2n - 1)\pi$ and $(2n + 1)\pi$ and the subsequent oscillation being about $2n\pi$. Eventually, however, as the initial velocity is successively reduced, a specific initial velocity will be reached for which the kinetic energy near the top of the circle (i.e., $\varphi = (2n - 1)\pi$) is just sufficient to enable the bead to reach the top and come to rest there. As the top is a position of unstable equilibrium, the bead cannot oscillate about that position, but must approach it uniformly from below. This is shown as curve B on sketch (c). For a slightly smaller initial velocity, the bead will not

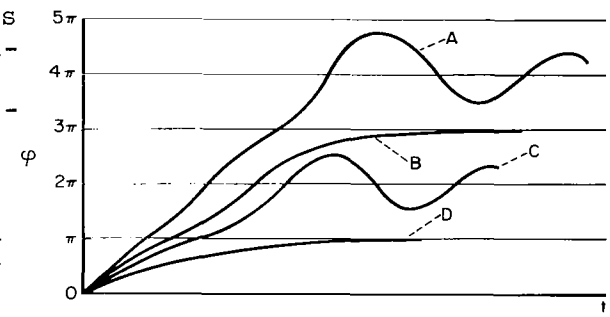

Sketch (c)

[1]It will be observed that this description of the arrest of tumbling does not entail the presence of aerodynamic damping. This contradicts a result presented in reference 8, in which the cause of the arrest of tumbling is attributed to a dissipation of rotational energy through aerodynamic damping. The author of reference 8 is led to this conclusion by the erroneous assumption that the net change of potential energy over one complete revolution is small enough to be neglected.

surmount the top and, hence, must oscillate about the next smaller multiple of 2π (i.e., $(2n - 2)\pi$). This is shown as curve C on sketch (c). Again, there will be a range of successively smaller initial velocities for which the bead will oscillate about $(2n - 2)\pi$, eventually terminating with an initial velocity that brings the bead to rest, without oscillating, at $(2n - 3)\pi$ (curve D).

To summarize this discussion as it applies now to the body, one observes that for any initial angle of attack α_i there will be a range of values of initial angular velocity $\dot{\alpha}_i$ that will cause α eventually to oscillate about a given value of $2n\pi$. This range of initial angular velocities is bounded by the two specific angular velocities which, for the same α_i, cause α to come to rest without oscillating at $(2n + 1)\pi$ and $(2n - 1)\pi$. The latter cases, where the body comes to rest in a position of unstable equilibrium, are somewhat unrealistic in practice. They can be important in analysis, however, as they serve to define the multiple of 2π about which α eventually oscillates.

Properties of the Transcendent

Although it is possible to obtain approximate analytical representations of the motions just described (cf. ref. 2), these solutions cannot be extended far enough to cover all cases of interest. In particular, they begin to fail as they approach the condition for which the body tends to dwell near a position of unstable equilibrium. On the other hand, it is not useful merely to present a catalog of numerical solutions for the Painlevé transcendent, as a separate solution would be necessary for each pair of initial conditions and this would require a prohibitive number of solutions. Alternatively, analysis can point the way to obtain a limited number of generalized numerical results from which most of the properties of interest can be derived. This will be the objective of the present section.

Definition of parameters.- Consider equation (11), and to bring in evidence that for the oscillatory solution, $\alpha \to 2n\pi$ as $x \to \infty$, let

$$\alpha = 2n\pi - 2\epsilon \tag{16}$$

where n is an integer, denoting the number of tumbles completed over the range of tumbling. As indicated in the preceding discussion, if its value is required, it must be determined from the nonoscillatory solution (cf. ref. 2). In the present study, however, it will not be necessary to know the cumulative value of α, but only its value relative to the final equilibrium position $2n\pi$. Hence, n need not be determined. It is convenient to retain the symbol α for designating angle of attack, but in doing so, henceforth we shall actually mean $\alpha - 2n\pi$, or interchangeably, -2ϵ. The equation of motion in terms of ϵ becomes

$$\epsilon'' + \frac{\epsilon'}{x} + \sin \epsilon \cos \epsilon = 0 \tag{17}$$

where now $\epsilon \to 0$ as $x \to \infty$. Consider a sequence of solutions of equation (17) in which the initial velocity $\epsilon'(\kappa)$ is held constant and $\epsilon(\kappa)$ is allowed to vary. A typical sequence is shown on sketch (d). Observe that for the given $\epsilon'(\kappa)$, there is a unique value of $\epsilon(\kappa)$ within an interval of π that will bring the motion to rest without oscillating at $\epsilon = -\pi/2$ (corresponding in α to an odd multiple of π). This motion is shown as curve A in sketch (d), and its initial value will be called the critical angle, $\epsilon_c(\kappa)$. It should be clear that the curve labelled B is identical to curve A and describes the same event, as do any two curves in ϵ whose initial velocities $\epsilon'(\kappa)$ are the same and whose initial values are separated by a multiple of π. As is evident from the sketch, all possible solutions for a given $\epsilon'(\kappa)$ are included within and bounded by the nonoscillatory solutions shown as curves A and B. Now in most applications, the questions of greatest interest will be: When does tumbling effectively stop and what is the nature of the subsequent oscillation? Both questions can be answered by defining conditions at the first peak of the oscillatory motion.[2] As shown on sketch (d), a locus of such points can be drawn which then intersects the first and largest peak of every one of the oscillatory motions. For any $\epsilon(\kappa)$ between ϵ_c and $\epsilon_c + \pi$, let ϵ_p be the value of ϵ at the first peak and $x(\epsilon_p)$ be the value of x at the first peak. Functionally, ϵ_p and $x(\epsilon_p)$ are dependent on the initial conditions; that is,

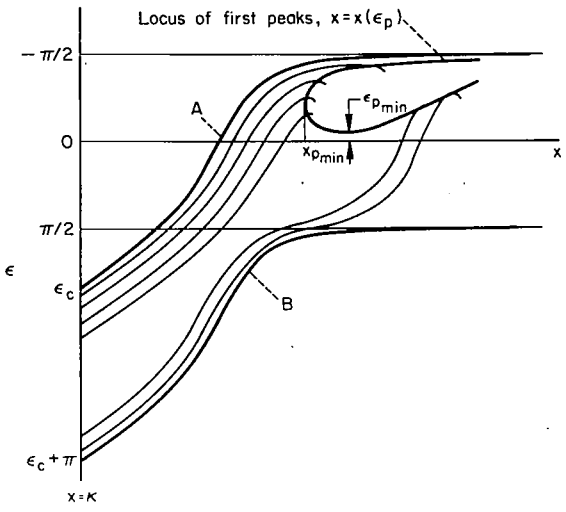

Sketch (d)

$$\left.\begin{aligned} \epsilon_p &= \epsilon_p(\epsilon(\kappa),\kappa\epsilon'(\kappa),\kappa) \\ x(\epsilon_p) &= x(\epsilon(\kappa),\kappa\epsilon'(\kappa),\kappa) \end{aligned}\right\} \tag{18}$$

For entry from without the atmosphere, for which $\kappa \to 0$, it can be shown that the functional relationships (18) no longer depend on κ. Further, it will be found convenient to show the dependence on $\epsilon(\kappa)$ as a dependence on an increment in $\epsilon(\kappa)$, the difference between $\epsilon(\kappa)$ and the critical angle ϵ_c. Thus, let

$$\Delta\epsilon_i = \epsilon(\kappa) - \epsilon_c \tag{19}$$

For entry from without the atmosphere, then

$$\left.\begin{aligned} \epsilon_p &= \epsilon_p(\dot{\alpha}_i/s,\Delta\epsilon_i) \\ x(\epsilon_p) &= x(\dot{\alpha}_i/s,\Delta\epsilon_i) \end{aligned}\right\} \tag{20}$$

---

[2]To be precise, tumbling actually stops earlier than at the first peak, namely, at the value of x for which $\epsilon'^2(x) = \cos^2 \epsilon$ (cf. ref. 2). However, the difference between the two coordinates generally is not great and the location of the first peak is a physically more tangible parameter to characterize the end of tumbling.

since

$$\kappa\epsilon'(\kappa) = -\dot{\alpha}_i/s$$

Note that these functional relationships are independent of all body parameters. They indicate the existence of single solutions applicable to all cases. Thus, it is practical to evaluate them numerically once and for all. This has been done and the results are presented on figures 1 and 2. In an entry from without the atmosphere, all values of $\Delta\epsilon_i$ are equally probable; however, the values of primary concern are those which lead to the largest first peaks of oscillation, for the subsequent oscillation amplitudes will

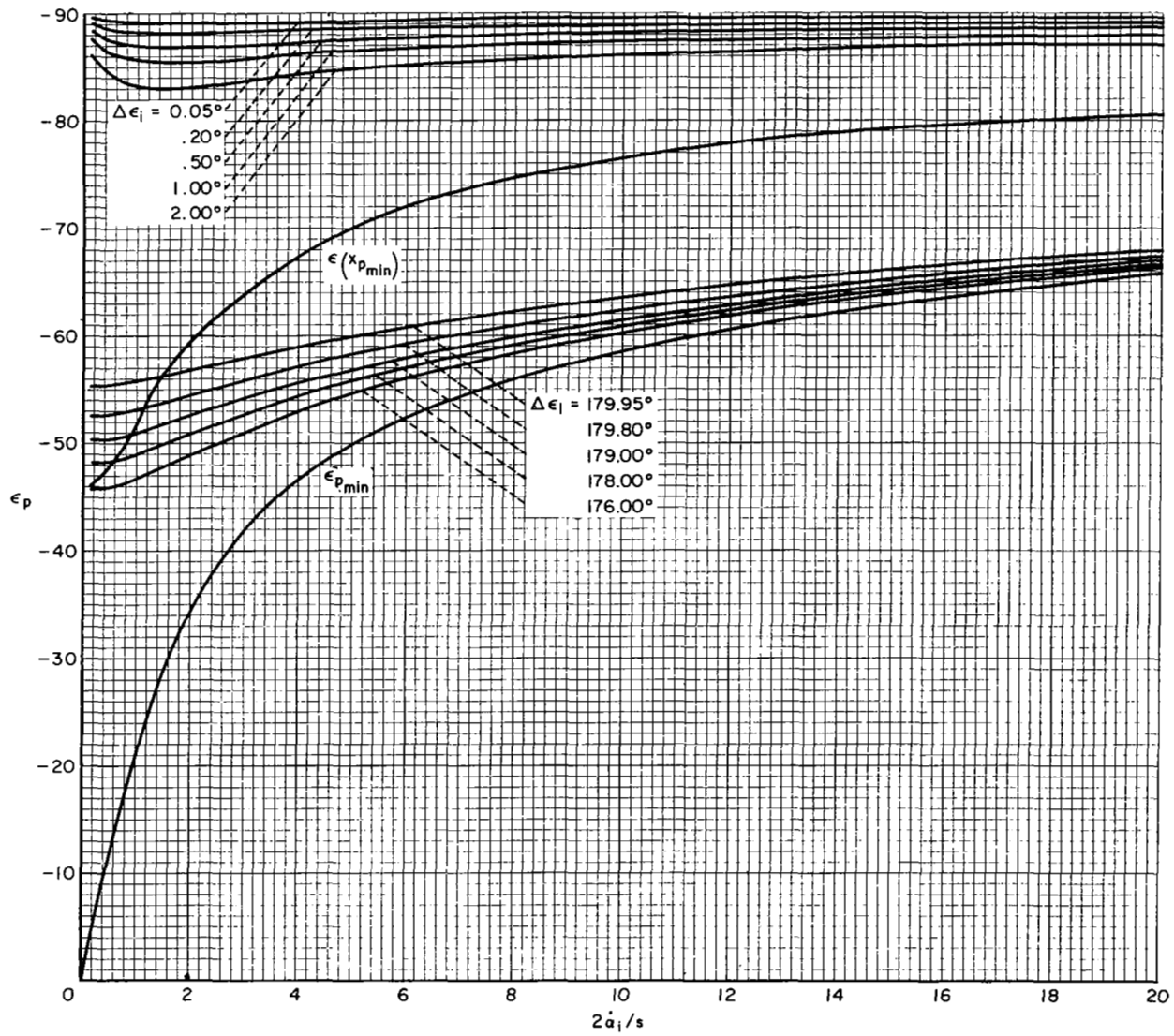

Figure 1.- Values of ϵ at the first peak of oscillation as a function of initial angular velocity.

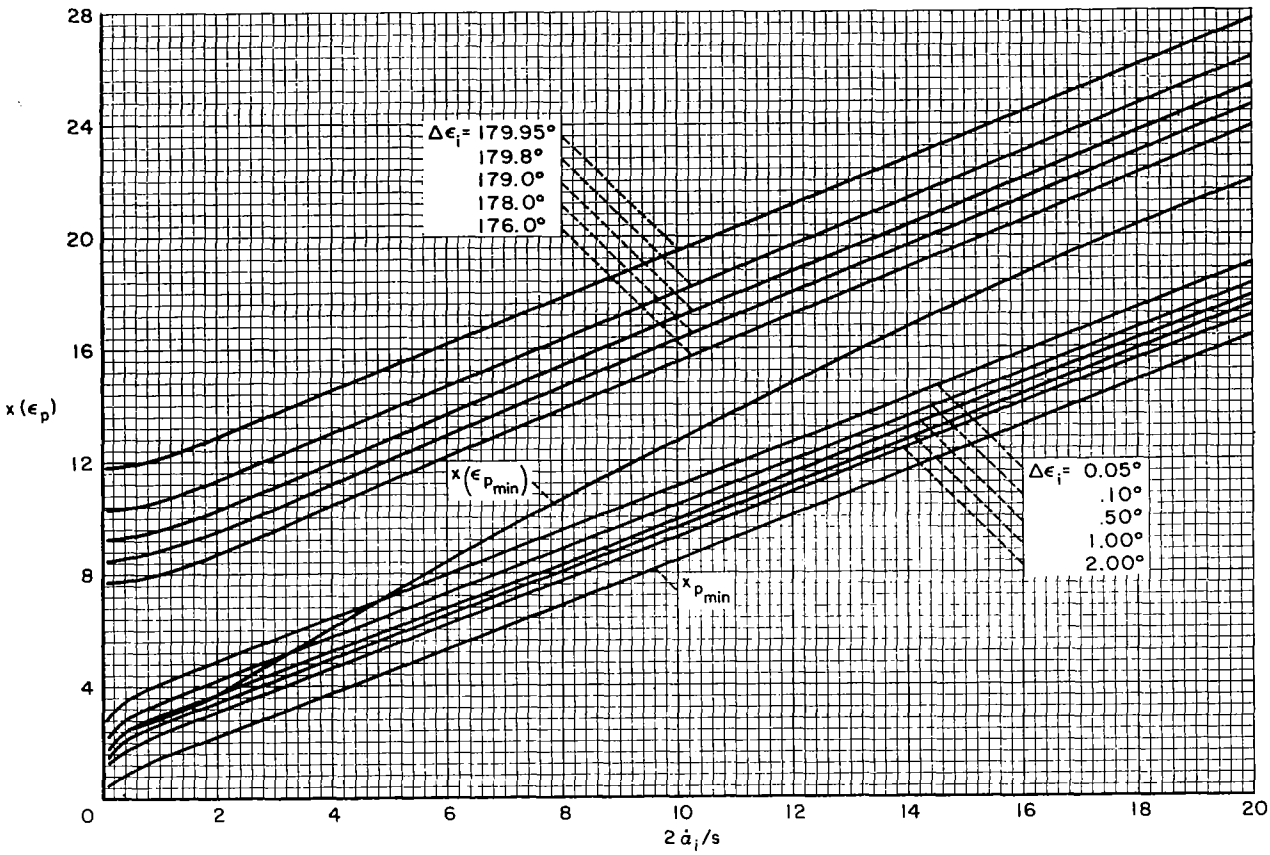

Figure 2.- Values of x at the first peak of oscillation as a function of initial angular velocity.

then be largest through the high heating and loading portions of the trajectory. Reference to sketch (d) will show that the largest first peaks occur when $\Delta\epsilon_i$ is near zero and again near π, and values of ϵ_p and $x(\epsilon_p)$ for these ranges of $\Delta\epsilon_i$ have been particularly stressed in figures 1 and 2. It will be seen also on sketch (d) that there exist two solutions of special significance. One of these gives the minimum possible value of x for which the first peak can occur. It is denoted by $x_{p_{min}}$ and $\epsilon(x_{p_{min}})$ on figures 1 and 2. The second special solution leads to the smallest possible value of ϵ at the first peak. It is denoted by $\epsilon_{p_{min}}$ and $x(\epsilon_{p_{min}})$ on figures 1 and 2. The latter solution is particularly important since, as will be shown, it may be used to establish a lower bound for the envelope of oscillatory motion. That this minimum angle of attack at the first peak of oscillatory motion must be different from zero will be evident when it is recalled that all of the rotational energy of the body must show up as potential energy due to angle of attack when the body pitch rate is zero.

Asymptotic solution for zero initial pitch rate.- With the magnitude and coordinate of the first peak of oscillatory motion defined, it is now possible to treat the oscillatory motion relatively simply. In effect, the problem has

been reduced to the case of a nontumbling body which begins its oscillatory motion at $x(\epsilon_p)$, a particular value of x, with the initial conditions $\epsilon_i = \epsilon_p$, $\epsilon_i' = 0$. Let $f = \tan \epsilon$. Equation (17) becomes

$$f'' - \frac{2ff'^2}{1 + f^2} + \frac{f'}{x} + f = 0 \tag{21}$$

Noting the resemblance of equation (21) to the equation for the Bessel function of zero order, one may cast equation (21) in the form of an integral equation involving the Bessel function by means of the method of variation of parameters. Thus,

$$f = \bar{Z}_o(x) + \frac{\pi}{2} \int_x^\infty \xi l(\xi)[J_o(x)Y_o(\xi) - Y_o(x)J_o(\xi)]d\xi \tag{22}$$

with

$$\left.\begin{aligned} l(x) &= \frac{2f(x)f'^2(x)}{1 + f^2(x)} \\ \bar{Z}_o(x) &= \bar{a}J_o(x) + \bar{b}Y_o(x) \\ \bar{a} &= a - \frac{\pi}{2} \int_{x(\epsilon_p)}^\infty \xi l(\xi)Y_o(\xi)d\xi \\ \bar{b} &= b + \frac{\pi}{2} \int_{x(\epsilon_p)}^\infty \xi l(\xi)J_o(\xi)d\xi \\ a &= -\frac{\pi}{2} x(\epsilon_p)Y_1(x(\epsilon_p)) \tan \epsilon_p \\ b &= \frac{\pi}{2} x(\epsilon_p)J_1(x(\epsilon_p)) \tan \epsilon_p \end{aligned}\right\} \tag{23}$$

The integral in equation (22) can be shown to diminish faster than $x^{-1/2}$ as $x \to \infty$, and hence the asymptotic behavior of $f(x)$ is $f(x) \sim \bar{Z}_o(x)$. Values of x in the portion of the trajectory of primary interest, where aerodynamic loads and heating become significant, are sufficiently large that the asymptotic behavior of $\bar{Z}_o(x)$ may be used. Then, for large x

$$f(x) \approx \frac{1}{\sqrt{x}} \sqrt{\frac{2}{\pi}(\bar{a}^2 + \bar{b}^2)} \sin\left(x - \frac{\pi}{4} + \mu\right) \tag{24}$$

where

$$\mu = \tan^{-1} \frac{\bar{a}}{\bar{b}}$$

The envelope of oscillation is given by

$$(\tan \epsilon)_{env} = \frac{1}{\sqrt{x}} \sqrt{\frac{2}{\pi} (\bar{a}^2 + \bar{b}^2)} \tag{25}$$

Since for small values of ϵ_p, $\bar{a} \to a$, $\bar{b} \to b$, it is convenient to normalize equation (25) as follows:

$$\frac{(\tan \epsilon)_{env}}{\sqrt{\frac{2}{\pi}(a^2 + b^2)}} = \frac{1}{\sqrt{x}} \sqrt{\frac{\bar{a}^2 + \bar{b}^2}{a^2 + b^2}} \tag{26}$$

Let

$$G = \sqrt{\frac{\bar{a}^2 + \bar{b}^2}{a^2 + b^2}}$$

where

$$G = G(\epsilon_p, x(\epsilon_p))$$

and

$$C = x(\epsilon_p) \sqrt{\frac{\pi}{2} \left[Y_1^2(x(\epsilon_p)) + J_1^2(x(\epsilon_p)) \right]}$$

where

$$C = C(x(\epsilon_p))$$

(27)

Then equation (26) takes the simple form

$$\frac{\sqrt{x}\,(\tan \epsilon)_{env}}{C \tan \epsilon_p} = G \tag{28}$$

Equation (28) is the correct asymptotic expression for the envelope curve of $\tan \epsilon$ in terms of the parameter G. Unfortunately, G cannot be evaluated analytically but since it is dependent upon only two parameters, ϵ_p and $x(\epsilon_p)$, it is practical to evaluate it numerically for a wide enough range to suffice for all conditions of interest. This has been done and the results are presented in figure 3.[3] For convenience, the parameter C has also been evaluated and the results are presented in figure 4. With G determined, equation (28) is a very general expression for the body's envelope of oscillatory motion. Observe that it is independent of all body parameters. It is specialized to a particular case by relating x to some physically significant parameter such as altitude, fraction of maximum dynamic pressure, or fraction of maximum aerodynamic heating. Examples of these relationships will be given in the next section.

---

[3]The origins of the curves for $x(\epsilon_p) = 10$ and $x(\epsilon_p) = 20$ have been displaced for clarity.

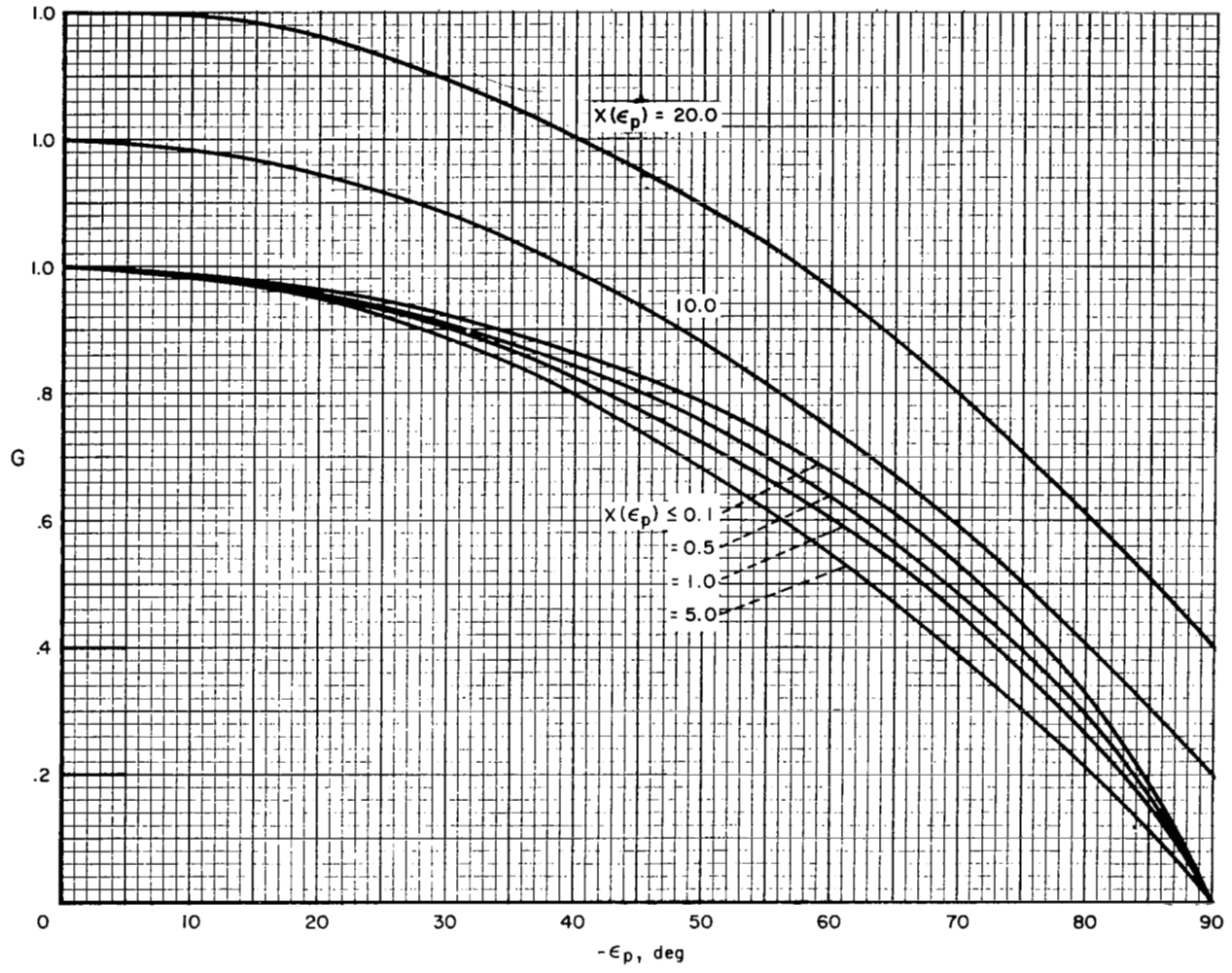

Figure 3.- Variation of the parameter G with ϵ_p for several values of $x(\epsilon_p)$.

Finally, consider the case $x(\epsilon_p) \to 0$, which corresponds to the nontumbling entry of a body from without the atmosphere. Inspection of the results of figure 3 shows G to be independent of $x(\epsilon_p)$ for values of $x(\epsilon_p)$ approaching zero. Further, C (eqs. (27)) is also independent of $x(\epsilon_p)$ for small $x(\epsilon_p)$, as may be shown when the Bessel functions in C are replaced with their initial behavior approximations. Thus,

$$C \to \sqrt{\frac{2}{\pi}} \quad \text{for} \quad x(\epsilon_p) \to 0 \tag{29}$$

With these results, equation (28) may be further simplified for the case of a nontumbling entry from without the atmosphere. The envelope of oscillatory motion is given by

$$(\tan \epsilon)_{env} = \sqrt{\frac{2}{\pi x}}\, G(\epsilon_p) \tan \epsilon_p \qquad (30)$$

It is of particular interest to note the general nature of the solution offered in equation (30). The solution written as a function of the coordinate x is independent of all body parameters, planetary properties, and initial conditions except initial angle of attack.

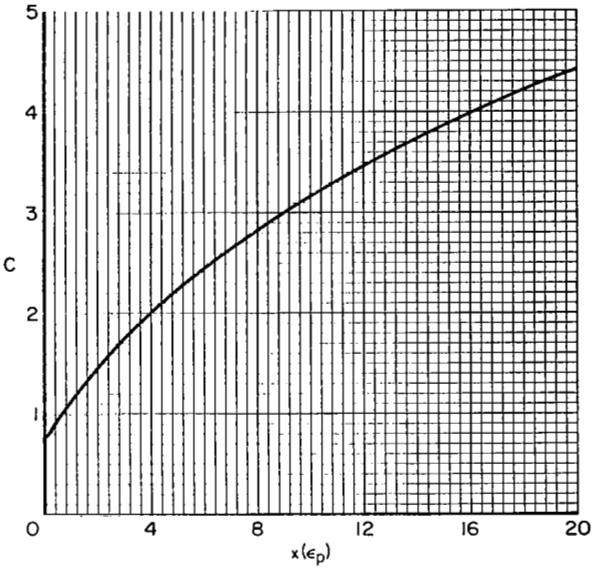

Figure 4.- Variation of the parameter C with $x(\epsilon_p)$.

Useful Relations

Within the assumptions of this analysis ($V = V_i, \gamma = \gamma_i$), the dynamic pressure varies as

$$q/q_i = e^{\beta V_i \sin \gamma_i t} \qquad (31)$$

Hence, from equations (10)

$$\frac{x}{\kappa} = \sqrt{\frac{q}{q_i}} \qquad (32)$$

so that the envelope expression (eq. (28)) may be rewritten

$$\frac{(\tan \epsilon)_{env}}{\tan \epsilon_p} = CG\kappa^{-1/2} \left(\frac{q}{q_i}\right)^{-1/4} \qquad (33)$$

It will be noted that this form is in agreement with the asymptotic form (for negligible aerodynamic damping) previously derived in reference 5 for the case of small initial α. The latter derivation is not dependent on assumptions concerning the variations of either flight-path angle or flight velocity. Hence, equation (33) can be extended, and the restrictions underlying its development circumvented, by the simple expedient of using a more precise expression for q/q_i in place of equation (31). The results of reference 9 are particularly useful in this regard as they permit one to write this ratio in a variety of forms involving physically significant parameters.

Envelope of oscillation in terms of altitude.- From reference 9

$$V = V_i e^{-(C_D \rho_o A/2\beta m \sin \gamma_i) e^{-\beta y}} \qquad (34)$$

so that

$$\frac{q}{q_i} = \frac{\rho_o V_i^2}{2q_i} e^{-\beta y} e^{-(C_D \rho_o A/\beta m \sin \gamma_i) e^{-\beta y}} \qquad (35)$$

Substituting equation (35) in (33) gives

$$\frac{(\tan \epsilon)_{env}}{\tan \epsilon_p} = CG\left[\frac{-\beta^2 \sin^2 \gamma_i I}{2\rho_o A l C_{m_{max}}} e^{\beta y_e}(C_D \rho_o A/\beta m \sin \gamma_i) e^{-\beta y}\right]^{1/4} \tag{36}$$

where

$$\epsilon_p = \epsilon_p(\dot{\alpha}_i/s, \Delta\epsilon_i) , \qquad C = C(x(\epsilon_p)) , \qquad G = G(\epsilon_p, x(\epsilon_p))$$

It should be kept in mind in using equation (36) that x has been assumed to be sufficiently large that the solution is indeed described by its asymptotic form. Thus, there is implied an upper bound on y which will exclude values of y large enough to cause $(\tan \epsilon)_{env}/\tan \epsilon_p$ to exceed or approach unity.

Envelope of oscillation in terms of dynamic pressure.- From reference 9 the maximum dynamic pressure is

$$q_{max} = \frac{1}{2e}\left(\frac{s^2}{\beta \sin \gamma_i}\right)\left(\frac{m}{C_D A}\right) \tag{37}$$

Writing q/q_i as

$$\frac{q}{q_i} = \frac{q}{q_{max}} \frac{q_{max}}{q_i} \tag{38}$$

and substituting equations (37) and (38) in (33) gives

$$\frac{(\tan \epsilon)_{env}}{\tan \epsilon_p} = CG\left[-\frac{1}{2}\left(\frac{I}{A l C_{m_{max}}}\right)(\beta e \sin \gamma_i)\left(\frac{C_D A}{m}\right)\frac{q_{max}}{q}\right]^{1/4} \tag{39}$$

Envelope of oscillation in terms of aerodynamic heating.- The results of reference 9 provide the following expression for fraction of maximum stagnation-point heating rate

$$\frac{\dot{H}_s}{(\dot{H}_s)_{max}} = e^{-\beta(\Delta y/2)_e}(1/2)(1-e^{-\beta \Delta y}) \tag{40}$$

where

$$\left.\begin{aligned} \Delta y &= y - y_1 \\ y_1 &= \text{altitude for maximum heating rate} \\ y_1 &= \frac{1}{\beta} \log\left(\frac{3 C_D \rho_o A}{\beta m \sin \gamma_i}\right) \end{aligned}\right\} \tag{41}$$

Equation (40) cannot be inverted to solve for Δy, so that a graphical solution is necessary. This is presented in reference 9. Substituting equations (41) in (36) gives

$$\frac{(\tan \epsilon)_{env}}{\tan \epsilon_p} = CG\left[-\frac{3}{2}\left(\frac{C_D A}{m}\right)(\beta \sin \gamma_i)\left(\frac{I}{A l C_{m_{max}}}\right) e^{\beta \Delta y} e^{(1/3) e^{-\beta \Delta y}}\right]^{1/4} \tag{42}$$

where $\beta \Delta y$ can be related to $\dot{H}_s/(\dot{H}_s)_{max}$ through the graphical solution provided in reference 9.

APPLICATIONS

As illustration of their use, the preceding results will be applied in two different connections; first, as an aid in the design of vehicles intended for use as planetary probes and, second, as an adjunct to the research into the origin of tektites. As a preliminary to both applications, however, a method will be presented that will be of general use in placing reasonable bounds on the oscillation envelopes of initially tumbling bodies.

Bounds on Oscillation Envelopes

A body making an uncontrolled entry into a planetary atmosphere generally will be tumbling at an essentially constant rate prior to entering the sensible atmosphere. Because of the tumbling motion, generally it will not be possible to specify the angle of attack at the precise moment aerodynamic effects begin to influence the motion. Therefore, an uncertainty in the angle-of-attack history within the atmosphere will necessarily prevail. However, it is possible to relate the parameters describing the body and its trajectory to the probability that the body will eventually undergo oscillations bounded by specified envelopes. Thus, the uncertainty in the angle-of-attack envelope history within a given atmosphere is bounded below by a minimum possible for a given initial tumbling rate and above by a maximum for which the probability of exceeding the maximum can be specified.

Consider first the lower bound. The results giving envelopes of oscillation in terms of aerodynamic heating and dynamic pressure may be put into a particularly convenient form. First, let

$$B = \left(\frac{C_D A}{m}\right)(\beta \sin \gamma_i)\left(\frac{I}{A l C_{m_{max}}}\right) \tag{43}$$

Then, with the use of equations (39) and (42), the values of the minimum possible envelopes evaluated at, respectively, maximum dynamic pressure and maximum heating may be given the form

$$\left.\begin{aligned}\left[(\tan\epsilon)_{\text{min env}}\right]_{\text{max q}} &= CG\left(-\frac{e}{2}B\right)^{1/4}\tan\epsilon_{p_{\min}}\\ \left[(\tan\epsilon)_{\text{min env}}\right]_{\text{max heat}} &= CG\left(-\frac{3}{2}e^{1/3}B\right)^{1/4}\tan\epsilon_{p_{\min}}\end{aligned}\right\} \qquad (44)$$

Note that, aside from the parameter B, equations (44) contain terms involving only the initial tumbling-rate parameter $2\dot{\alpha}_i/s$. Thus, if values of B are chosen for a wide enough range to cover all cases of interest, these relations may be evaluated once and for all. The results are presented on figure 5. Now, it is further noted that the following relations hold

$$\left.\begin{aligned}\frac{(\tan\epsilon)_{\text{min env}}}{\left[(\tan\epsilon)_{\text{min env}}\right]_{\text{max q}}} &= \left(\frac{q_{\max}}{q}\right)^{1/4}\\ \frac{(\tan\epsilon)_{\text{min env}}}{\left[(\tan\epsilon)_{\text{min env}}\right]_{\text{max heat}}} &= \left[\frac{e^{\beta\Delta y}e^{(1/3)e^{-\beta\Delta y}}}{e^{1/3}}\right]^{1/4}\end{aligned}\right\} \qquad (45)$$

and that these expressions are independent of all parameters relating to the body. These functions are presented graphically in figure 6. The minimum possible envelope of oscillation in terms of fraction of maximum dynamic pressure or fraction of maximum heating can be computed from the graphs of figures 5 and 6. A relationship between the minimum envelopes and envelopes having a specified probability of being exceeded will now be established.

A study of sketch (d), for a given initial tumbling rate, suggests the possibility that the asymptotic behavior of the envelopes of oscillatory motion for two different initial angles of attack might be identical. Inspection of equation (28) reveals that this will indeed be the case if the term CG tan ϵ_p is the same for two different initial angles of attack. Now it is noted that this product is a function only of $\Delta\epsilon_i$ for a given tumbling rate and that for each value it takes on for $\Delta\epsilon_i$ near zero there is a corresponding $\Delta\epsilon_i$ near π for which it has the same value. Values of $\Delta\epsilon_i$ near zero correspond physically to the body being oriented in an attitude slightly less inclined to the stream than the critical attitude and values of $\Delta\epsilon_i$ near π correspond to the body being at a slightly greater inclination than for the critical; an appropriate interpretation of these values gives the probability of exceeding a particular envelope. Thus, suppose that a particular value of CG tan ϵ_p is chosen and that this same value results from both $\Delta\epsilon_i = 1.5^\circ$ and $\Delta\epsilon_i = 179.5^\circ$. For values of $\Delta\epsilon_i$ between 0° and 1.5°, or between 179.5° and 180°, the subsequent envelopes of oscillation will exceed those for all $\Delta\epsilon_i$ between 1.5° and 179.5°. Then there is a 2.0° range of $\Delta\epsilon_i$ out of a possible 180° range, or a probability of 1/90 that the envelope for the chosen value of CG tan ϵ_p will be exceeded.

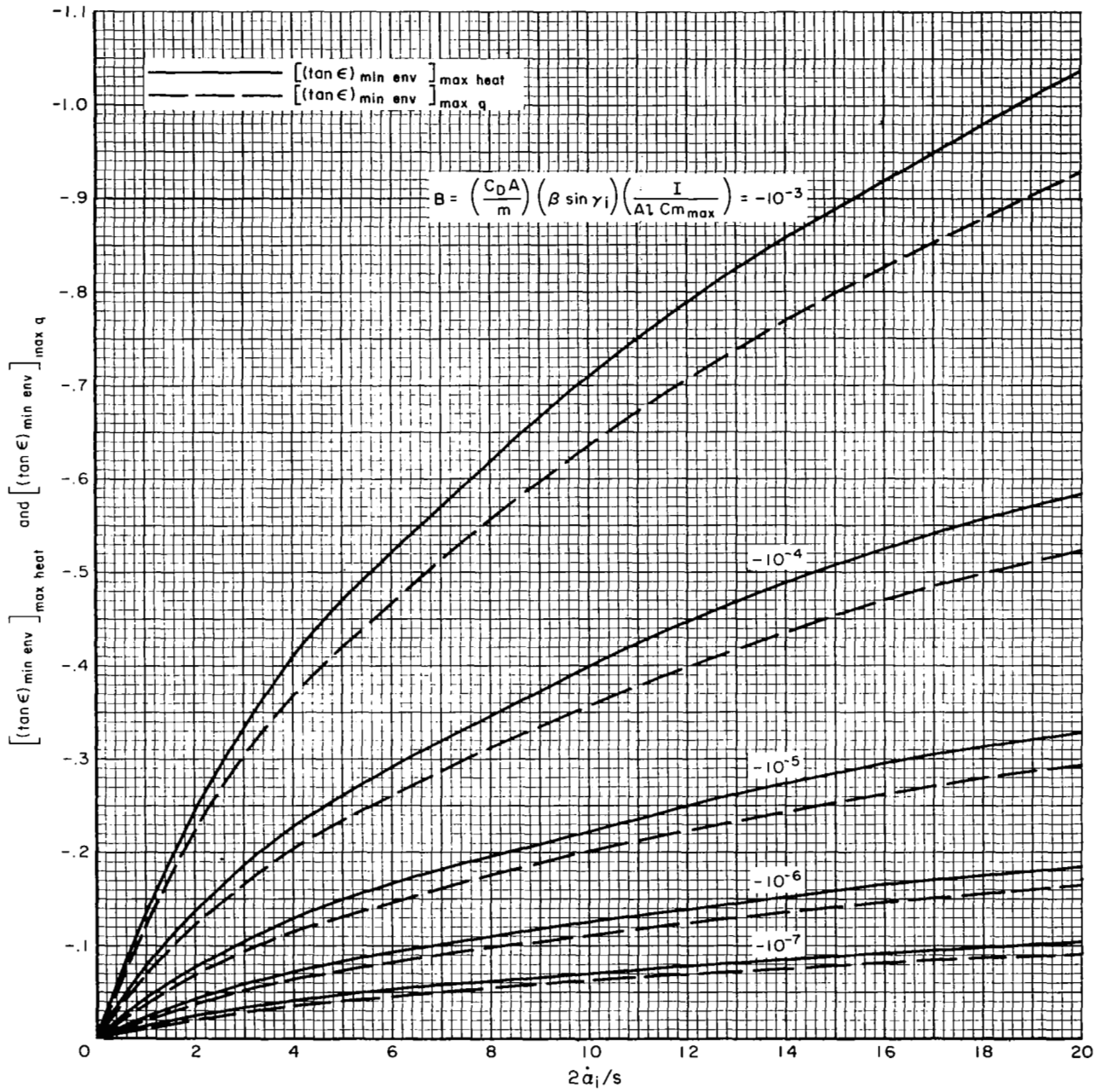

Figure 5.- Minimum possible envelope values of tan ϵ at maximum heating and maximum dynamic pressure as functions of initial angular velocity for several values of the parameter B.

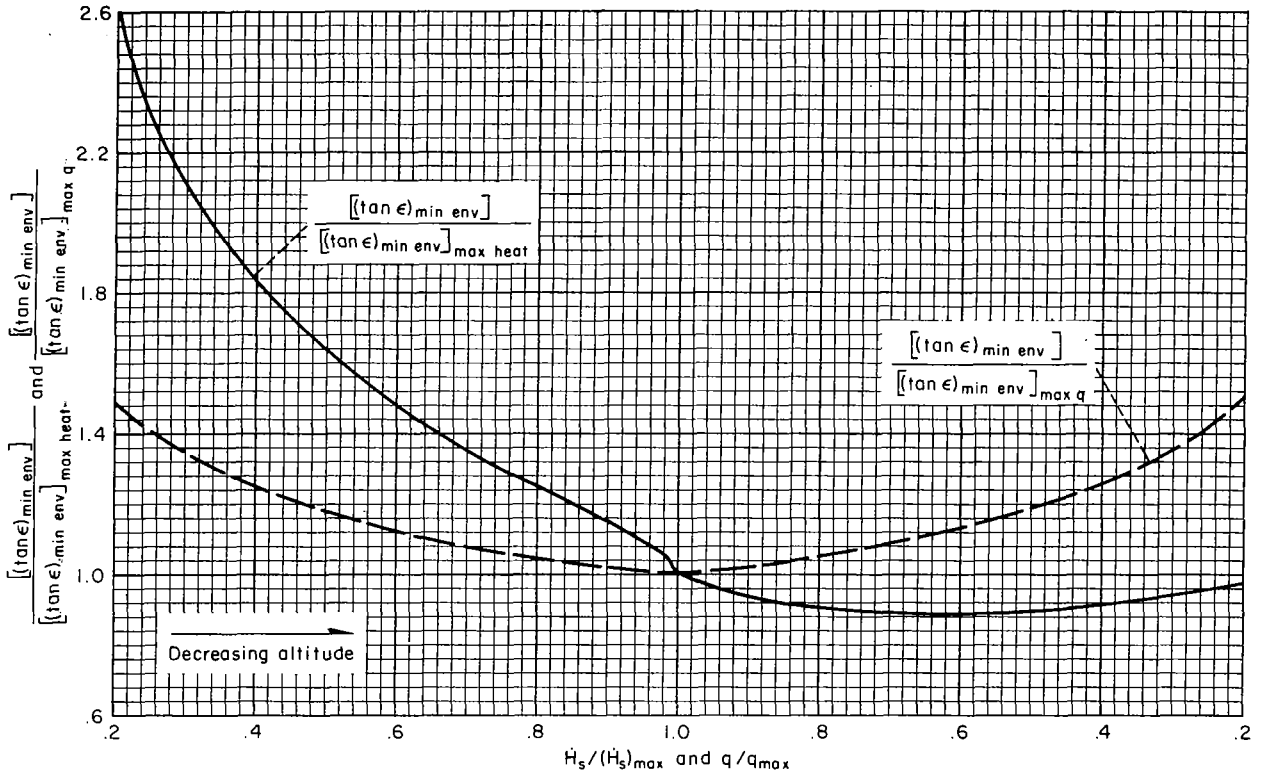

Figure 6.- Relationship between minimum possible envelope values of tan ϵ and fraction of maximum heating and maximum dynamic pressure.

The relationship between an envelope of oscillation having a specified probability of being exceeded and the minimum possible envelope is independent of the characteristics of the body. One observes this by forming the following ratio, using equation (28)

$$\frac{(\tan\epsilon)_{env}}{(\tan\epsilon)_{min\ env}} = \frac{C(\epsilon_p)G(\epsilon_p, x(\epsilon_p))\tan\epsilon_p}{C\left(\epsilon_{p_{min}}\right)G\left(\epsilon_{p_{min}}, x\left(\epsilon_{p_{min}}\right)\right)\tan\epsilon_{p_{min}}} \tag{46}$$

and noting that the right side is dependent only upon the tumbling rate parameter $2\dot{\alpha}_i/s$. This relationship has been evaluated for several probabilities and the results are presented on figure 7. Application of the results of figures 5, 6, and 7 to make estimates of the upper and lower bounds to the envelope of oscillation is illustrated in the following section.

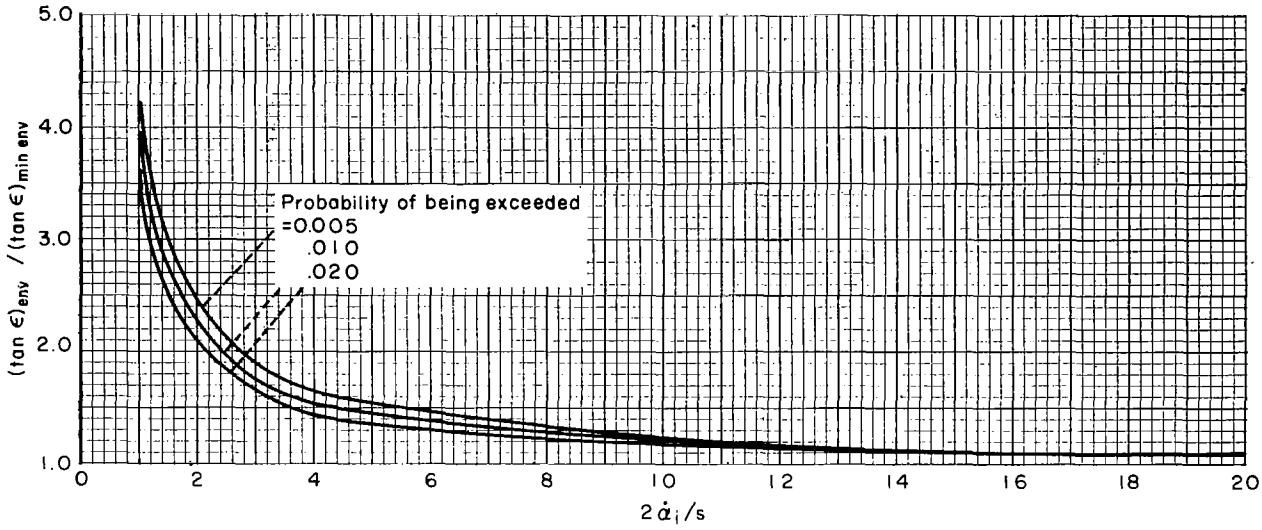

Figure 7.- Relationship between envelope values of tan ϵ having a specified probability of being exceeded and values of tan ϵ for the minimum possible envelope as a function of initial angular velocity.

Motions of Planetary Probe Vehicles

To illustrate the use of the results and to assess their accuracy, a sample calculation will be made and compared with results in which no approximations were made either to the equations of motion or to the aerodynamic forces and moments. The comparison will be made with the results of reference 1 for a vehicle making a tumbling entry into the martian atmosphere.

Calculation of parameters.- The vehicle studied in reference 1 had the following physical properties:

$$A = 8.296 \text{ ft}^2$$

$$I = 5.6 \text{ lb-ft-sec}^2$$

$$l = 3.25 \text{ ft}$$

$$m = 6.685 \text{ lb-sec}^2/\text{ft}$$

$$C_D = 0.650$$

$$C_{m_{max}} = -0.162$$

where $C_{m_{max}}$ was evaluated so that the area under a half-cycle of the approximating sine function curve equalled that under the actual pitching-moment variation. The martian atmosphere and the entry conditions were given as

$$\beta = 2.15\times10^{-5}/\text{ft}$$
$$V_i = 21{,}042 \text{ ft/sec}$$
$$\gamma_i = 41.5^\circ$$
$$\dot{\alpha}_i = 0.2094 \text{ radian/sec}$$

leading to

$$s = 0.30/\text{sec}$$
$$2\dot{\alpha}_i/s = 1.396$$
$$B = -1.432\times10^{-5}$$

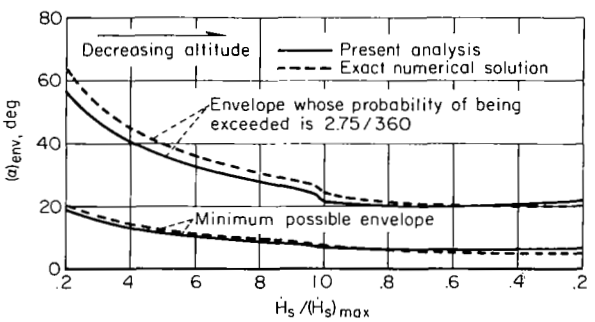

Figure 8.- Envelopes of oscillatory motion as a function of fraction of maximum heating rate for a Mars entry; initial angular velocity = 12°/sec.

Determination of angle-of-attack envelopes.- The minimum possible envelope of oscillatory motion in terms of aerodynamic heating rate, subsequent to the arrest of tumbling, is determined in the following way: Enter figure 5 with the given values of $2\alpha_i/s$ and B to obtain $[(\tan \epsilon)_{\text{min env}}]_{\text{max heat}}$. Use this value in conjunction with figure 6 to construct a graph of $(\alpha)_{\text{min env}}$ versus $\dot{H}_s/\dot{H}_{s_{max}}$. Results of this calculation are presented on figure 8 and the exact results are shown for comparison. One obtains the envelope having a probability of 2.75/360 of being exceeded by entering figure 7 with the given values of $2\dot{\alpha}_i/s$ and probability; this gives the ratio of the envelope values of the upper and lower bounds of $\tan \epsilon$. The upper bound envelope is constructed from the product of this ratio and the already obtained minimum envelope. Results of this calculation are also shown on figure 8 and compared with the exact results. It is noted that the agreement between the exact result and that of the present theory is within 10 percent throughout.

Motions of Tektites

Origin of tektites.- From the exhaustive studies of the nature of the curious glass objects known as tektites (see ref. 4 for an extensive bibliography), it has been known for a long time that the tektites experienced two separate periods of intense heating. During the first, heating was sufficiently intense to melt the objects completely, whereas in the second, heating was sufficient only to melt the thin surface layers of otherwise solid objects. After the extensive investigations of Chapman and his colleagues (refs. 4 and 10), in which the ring-wave markings and coiled flanges that are such distinctive features of the Australian tektites were reproduced with fidelity in wind-tunnel experiments, there can be little doubt that the second period of melting occurred as the result of a hypervelocity passage through the Earth's

atmosphere. Further, from a minute study of the striae lying beneath the tektites' surfaces, combined with the observed final tektite geometry, the authors of references 4 and 10 have been able to deduce the probable speed and flight-path angle of these objects as they entered the atmosphere, and they have concluded that the entry conditions deduced were compatible with those for objects whose origin was the Moon. If this conclusion is accepted as correct, the following sequence of events may be hypothesized: The Moon is struck by a meteor, the lunar surface at the point of impact is vaporized and streams of molten lunar surface material are ejected outward from the crater at very great velocity, at such great velocity indeed that the molten material has sufficient kinetic energy to escape the gravitational field of the Moon. Subsequently, some of the lunar material traverses a path in space that brings it within a corridor permitting capture by the Earth's gravitational field. Sometime after its ejection from the Moon, the stream of molten material breaks into segments which tend to contract into characteristic shapes by the action of surface tension, congeal, and solidify as they lose their heat by radiation. The tektites then enter the Earth's atmosphere as solid bodies, and, during their passage through the atmosphere, acquire by ablative melting the characteristic ring waves and flanges that so distinguish them when they are found on the Earth's surface.

Now, if this sequence did actually originate with a collision, it seems probable that at least a portion of the lunar material should have acquired a certain amount of angular momentum. The molten objects then would have found themselves turning while in space and would have sought to assume the stable figures consistent with their turning rates. They would have been turning, or tumbling, also as they entered the Earth's atmosphere, but at least the Australian tektites with few exceptions could not have been either tumbling or oscillating with large amplitude during the period of greatest heating or the patterns characteristic of ablation on bodies with fixed orientation would not be present on the many existing specimens. Therefore, their tumbling motion had to have been arrested and their subsequent oscillatory motion reduced to quite small amplitudes before their period of greatest heating, and it is the consequences of this requirement that can be studied by means of the present analysis.

Figures of equilibrium.- In order to apply the results of the preceding sections, a value of initial angular velocity must be assigned to the body. Further, the body shape should be chosen to be compatible with the assigned value of angular velocity, for, as mentioned above, the body in its molten state will tend to assume a figure consistent with its turning rate. Let it be assumed first that the viscosity of the body in its molten state is sufficiently low to permit the stable figure to be attained before the body solidifies.[4] The form attained may then be calculated. In effect, the problem is analogous to the famous problem in cosmogony of determining the figure of equilibrium of a rotating liquid mass (cf., e.g., ref. 12) except that the force tending to contract the mass is surface tension rather than gravitation (it is easy to show that for bodies the size of tektites the mutual attraction

[4]It is probable that this was the case only for the tektites found in the part of the strewnfield covering southeast Australia (cf. ref. 11). The succeeding analysis is therefore limited to that particular group of tektites.

of the bodies' particles is negligible compared with the surface tension force). The definitive analysis is due to Charrueau (ref. 13), but its essentials are repeated more accessibly in volume 4 of Appell's treatise on rational mechanics (ref. 14). For present purposes, it suffices to note the following results:

(1) In the absence of gravitation, the figure of equilibrium must have cylindrical symmetry; that is, cross sections normal to the axis of rotation are circles.

(2) The meridian curve for the figure of equilibrium is an elliptic function dependent on a single parameter K^2 having the form

$$K^2 = \delta\omega^2 a^3/8f \tag{47}$$

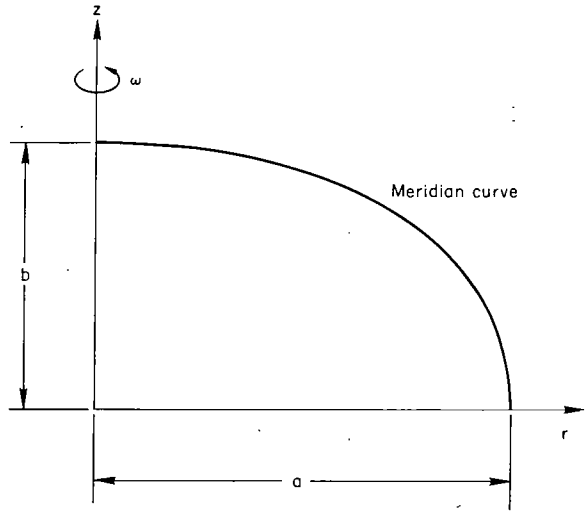

Sketch (e)

where

δ liquid density

ω angular velocity

f surface tension

a radius of figure in equatorial plane (see sketch (e))

(3) For $K^2 = 0$, that is, for zero turning rate, the figure of equilibrium is a sphere. Let its mass be m and its radius R. A body of the same mass with a small turning rate will flatten at its poles. For $K^2 \ll 1$, it is essentially an ellipsoid of revolution. The meridian curve z(r) (see sketch (e)) is approximately

$$z \approx (1 - K^2)\sqrt{a^2 - r^2}\ ; \qquad K^2 \ll 1 \tag{48}$$

where, for the same mass m, a and b, the semiaxes of the ellipse, are related to R by

$$\left.\begin{aligned} a &\approx R\left[1 + \frac{K^2}{3}\left(\frac{R}{a}\right)^3\right] \\ b &\approx R\left[1 - \frac{2}{3}K^2\left(\frac{R}{a}\right)^3\right] \end{aligned}\right\} \tag{49}$$

and the mass and the moment of inertia about the axis are, respectively,

$$\left.\begin{aligned} m &\approx \frac{4\pi}{3}(1 - K^2)a^3\delta \\ I_z &\approx \frac{2}{5}ma^2 \end{aligned}\right\} \qquad (50)$$

(4) For increasing values of K^2 the figure flattens progressively. In the absence of an external pressure, however (i.e., no atmosphere), the figure must remain convex and this requires $K^2 \leq 1$. The value $K^2 = 1$ therefore constitutes an upper bound on turning rate for which the body will seek cylindrical symmetry while in space. At this condition, for the same mass m, $a/R = 2^{1/3}$, $b/R = 0.543$. The exact forms of the figures of equilibrium over the whole range of K^2 from 0 to 1 are shown on figure 9.

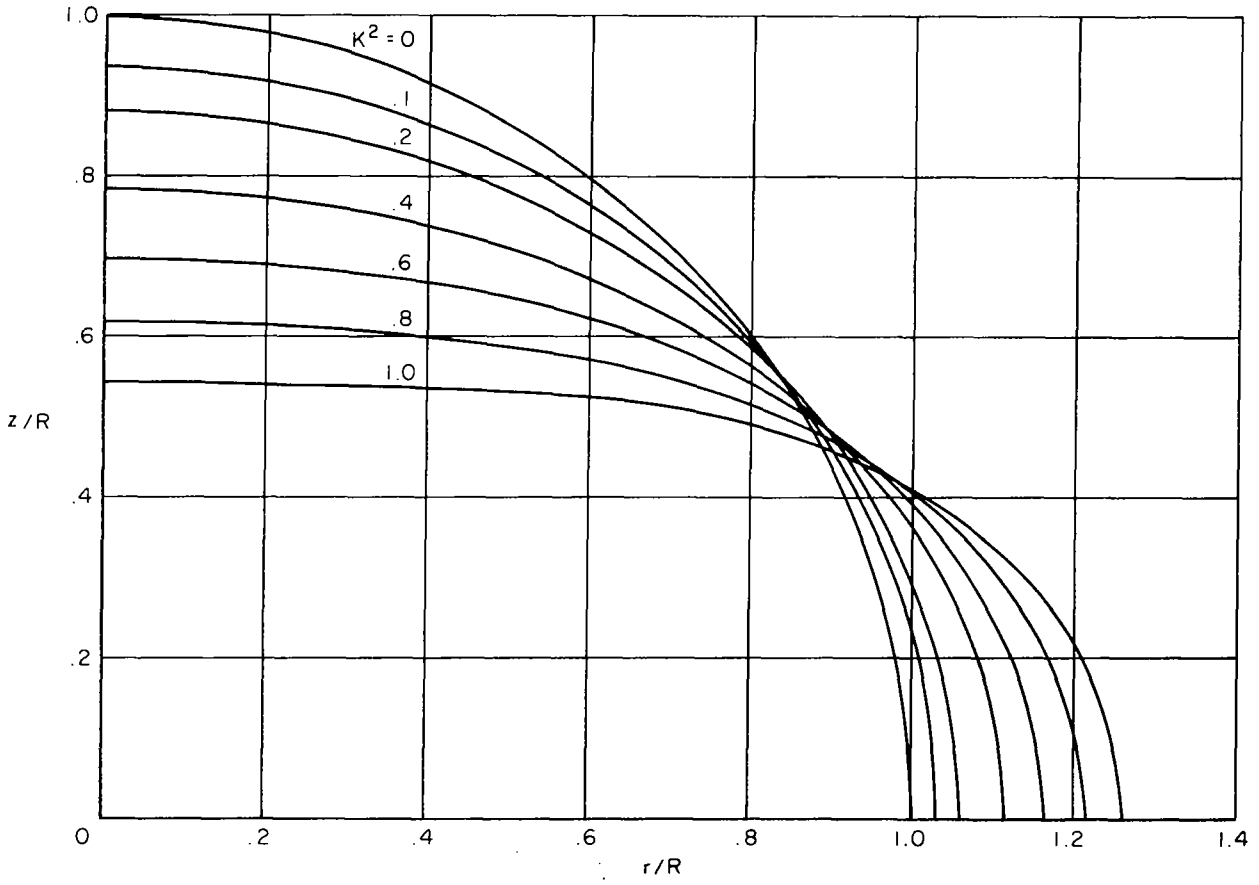

Figure 9.- Meridian curves of figures of equilibrium for a rotating liquid having the fixed mass of a sphere of radius R under the action of surface tension.

(5) In the absence of an external pressure, there are no figures of equilibrium for $K^2 > 1$. Presumably in this case the body will decelerate through a progression of elongating pear-shaped figures culminating in separation at the weakest section.

In application to tektites, it remains to assign representative numerical values to the physical properties appearing in the parameter K^2. These may be obtained from results given in reference 4. The density δ of tektite glass is given as 2.4 gm/cm^3. The surface tension f for glass of tektite composition is reported as 360 dynes/cm. A single representative mass will be assumed and will be taken to be that for a sphere of 1-cm radius. With these numbers, the limiting values of ω and angular momentum for which cylindrical symmetry is sought ($K^2 = 1$) are, respectively, the order of 25 radians/sec and 167 dyne-cm-sec.

Probability of a tumbling entry.- It has been assumed that the body attains a figure of equilibrium in space before it solidifies. As a consequence, it must rotate at a constant angular velocity about an axis through its center of gravity, and that axis must maintain a fixed attitude with respect to space-fixed coordinates (ref. 14). Hence, the angular velocity vector also maintains a fixed inclination with respect to the velocity vector and the body enters the atmosphere in this condition. An inclination of exactly 90° corresponds to a tumbling entry as defined here, whereas an inclination of 0° corresponds to a rolling motion around the velocity vector. Consider first the consequences of a purely tumbling entry for a figure of equilibrium, that is, for a body having cylindrical symmetry about the axis of rotation, the latter being inclined 90° to the stream. As shown on sketch (f), the aerodynamic force on the body always remains parallel to the velocity vector and passes through the body's center of volume. Barring the existence of a significant inhomogeneity or asymmetry, the center of gravity is coincident with the center of volume and the aerodynamic restoring moment about the center of gravity is identically zero. Hence, the body in this mode is in a state of unstable equilibrium; a disturbing force whose moment vector is even slightly misalined with the angular velocity vector will cause the body to depart from this mode and seek a new state of motion in which it is stable. Now consider a case in which the axis of rotation is inclined to the velocity vector at an angle less than 90°. Sketch (g) shows a view of the body in the plane containing both the axis of rotation and the velocity vector. As the body has cylindrical symmetry about the axis of rotation, its projection in this plane is invariant with time; the profile is approximately elliptical as a result of the flattening the body has undergone while turning in the liquid state. The aerodynamic force on the body lies wholly and continually in the plane; it is approximately alined with the stream, but passes through a point representative of

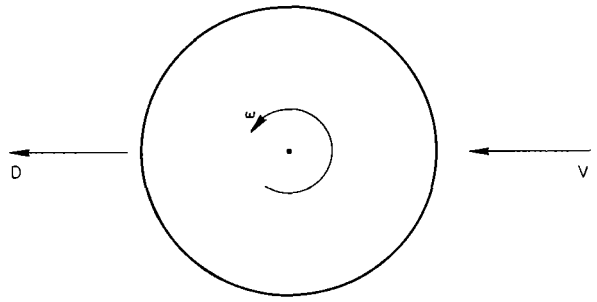

Sketch (f)

the center of curvature of the forward surface, a point which lies behind the center of gravity. It is clear that in this case an aerodynamic restoring moment is developed about the center of gravity that will drive the angle of attack σ toward zero. These considerations make it evident that the probability that a figure of equilibrium will undergo a tumbling entry is very remote. The stable state is with the cylindrical surface broadside to the stream, and for all initial inclinations other than exactly 90°, the body will tend to this state.

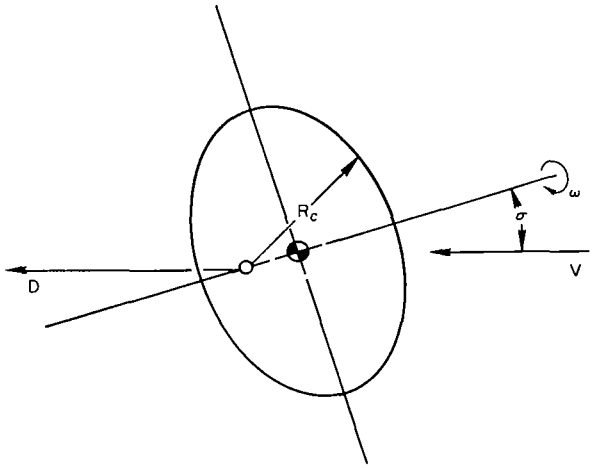

Sketch (g)

Nonplanar motions.- With tumbling effectively eliminated as the normal mode of entry for bodies which are figures of equilibrium, consideration must be given to nonplanar motions in which the angular velocity vector is initially fixed in space, inclined to the velocity vector at some angle less than 90°. It is possible, however, to relate this study in a simple fashion to results already obtained here.

In reference 15, Leon treated the problem of a spinning body entering the atmosphere, but under the restriction that the initial inclination of the angular velocity vector from the velocity vector be small. As initial inclinations up to 90° are of interest here, the results of reference 15 are of only limited applicability in the present context. A means of removing this limitation has been found; however, as it is suggested by the form of the results presented in reference 15, these will be reviewed briefly before their extension is presented. A sketch of the relevant coordinates, adopted from reference 15, is shown in sketch (h). The most important angle is σ, the inclination of the body axis z about which the body rotates, to the velocity vector along Z. As the body has cylindrical symmetry about the z axis, the aerodynamic force on the body is a function only of σ and lies in the σ plane. The aerodynamic moment about the center of gravity therefore lies on an axis normal to the σ plane, or along the line of nodes. The

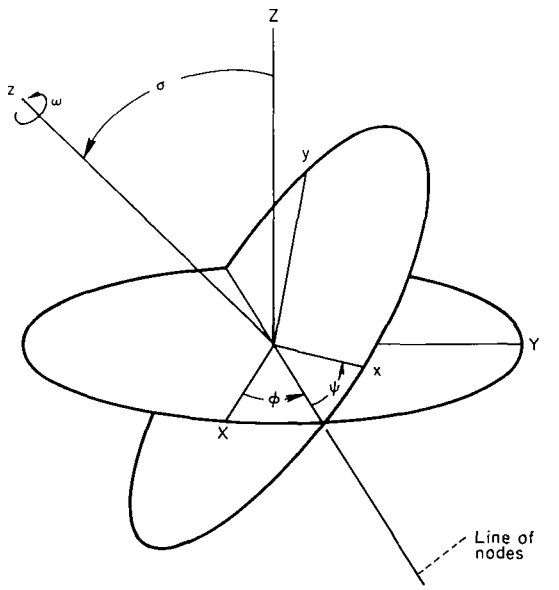

Z Flight path direction
z Body axis of rotation
σ Resultant angle of attack

Sketch (h)

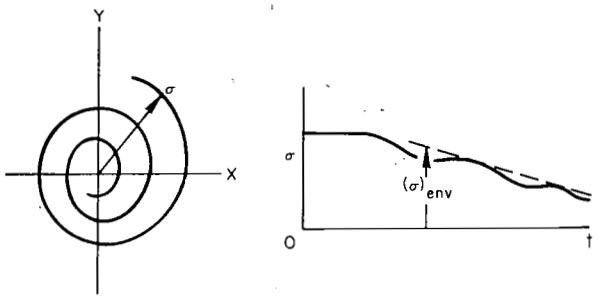

Sketch (i)

angle σ in effect defines the movement of the nose of the body about the velocity vector. In space and on entry into the atmosphere σ is fixed in value and orientation, but as the aerodynamic moment grows, the σ plane will begin to rotate about Z causing the body nose to move in a diminishing spiral. A typical σ history is shown on sketch (i) both as it appears to an observer on the Z axis and as a function of time. A very useful relation is found in reference 15, namely, the ratio between the asymptotic behavior of the envelope of σ, $(\sigma)_{env}$, (cf. sketch (i)) to the asymptotic behavior of the envelope of α for a planar, nonspinning, nontumbling entry. For the same entry conditions ($\sigma_i = \alpha_i$, $\dot{\sigma}_i = \dot{\alpha}_i = 0$), the ratio is simply

$$\frac{(\sigma)_{env}}{(\alpha)_{env}} = \sqrt{\frac{\pi\nu/2}{\tanh(\pi\nu/2)}} \tag{51}$$

where

$$\nu = \frac{\omega}{s}\frac{I_Z}{I}$$

Thus, it is indicated that the ratio of the envelopes is a constant and is increased by a factor dependent only on a single parameter ν.

The simple form of equation (51) suggested the possibility that a similar form would result even with the removal of the limitation to small values of σ_i. This has been found to be the case. When the aerodynamic restoring-moment coefficient can be expressed as $C_{m_{max}} \sin\sigma$, the extension of equation (51) to the case of arbitrarily large values of σ_i is of the form

$$\frac{(\tan\sigma/2)_{env}}{(\tan\alpha/2)_{env}} = \sqrt{\frac{\pi\bar{\nu}/2}{\tanh\pi\bar{\nu}/2}}\,\frac{G(\sigma_i,\nu)}{G(\sigma_i,0)}\;; \quad \bar{\nu} = \nu\cos^2\sigma_i/2 \tag{52}$$

In the present study, only small to moderate values of ν need be considered, and in this case the ratio involving G is essentially unity. Then, as before, the ratio of the envelopes is increased by a simple factor dependent only on $\bar{\nu}$. As the planar solution is already available (eq. (30)), equation (52) provides a simple means of studying the angle-of-attack behavior of rotating bodies having cylindrical symmetry about the axis of rotation. In effect, one need only study the simplest of planar problems, nontumbling entry from without the atmosphere; multiplying the result by the factor in equation (52) then gives the desired property of the rotating body.

In this light, consider the nontumbling planar entry of the figure of equilibrium with its cylindrical surface facing the stream. On sketch (j), a figure of equilibrium is shown superimposed on a sphere of the same mass so that their front faces are alined as nearly as possible. If the front face of the figure of equilibrium could be alined perfectly with that of the sphere, it is clear that the moment about the center of gravity of the figure of equilibrium would be of the form

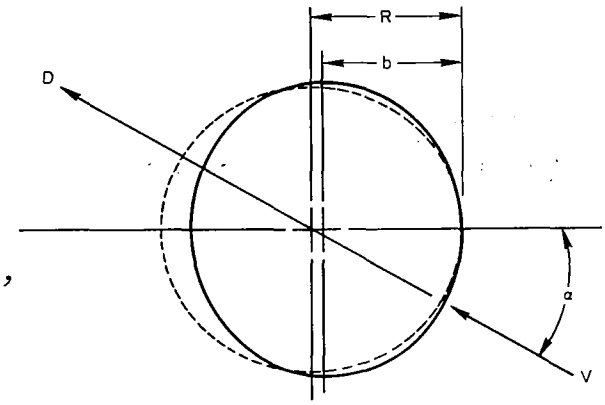

Sketch (j)

$$C_m = -C_D\left(\frac{R - b}{l}\right) \sin \alpha \qquad (53)$$

It is indicated, therefore, that for small amounts of oblateness equation (53) should adequately represent the pitching moment for the figure of equilibrium. On the other hand, because of the fore-and-aft symmetry of the figure, the pitching moment must be zero at $\alpha = \pi/2$, so that equation (53) will not apply for values of α in the immediate vicinity of $\pi/2$. With this range excluded, equation (53) is applicable to the figure of equilibrium having small oblateness. Hence, with C_m of the required form, equation (30) is applicable and is rewritten here for convenience

$$\frac{(\tan \epsilon)_{env}}{\tan \epsilon_p} = \sqrt{\frac{2}{\pi x}}\, G(\epsilon_p) \qquad (54)$$

where $\epsilon = -\alpha/2$. It is convenient to rewrite equation (54) in terms of the ratio q/q_{mh}, where q_{mh} is the dynamic pressure at maximum heating. We have from equation (32)

$$x^2 = \kappa^2 \frac{q}{q_i} = \kappa^2\left(\frac{q}{q_{mh}}\right)\frac{q_{mh}}{q_i} \qquad (55)$$

From equations (35) and (41)

$$q_{mh} = \frac{1}{6} e^{-1/3} V_i^2 \beta \sin \gamma_i \left(\frac{m}{C_D A}\right) \qquad (56)$$

so that x^2 becomes, when equations (10), (53), (55), and (56) are used,

$$x^2 = \frac{2}{3} e^{-1/3} \frac{1}{\beta \sin \gamma_i} (R - b) \frac{m}{I}\left(\frac{q}{q_{mh}}\right) \qquad (57)$$

As only small amounts of oblateness are admissible, the figure of equilibrium is essentially an ellipsoid of revolution for which the expressions for m and b previously presented (eqs. (47) through (50)) may be used. Retaining terms

only to the first order in K^2 gives

$$(R - b)\frac{m}{I} \approx \frac{5}{3}\frac{K^2}{R} \; ; \qquad K^2 \ll 1 \tag{58}$$

which relates the geometric properties of the body to the rotation parameter K^2. The envelope expression (eq. (54)) becomes

$$\frac{(\tan \epsilon)_{env}}{\tan \epsilon_p} = \sqrt{\frac{2}{\pi}}\, G(\epsilon_p)\, \frac{1}{\left(\frac{10}{9}\, e^{-1/3}\, \frac{K^2}{\beta R \sin \gamma_i}\right)^{1/4} \left(\frac{q}{q_{mh}}\right)^{1/4}} \tag{59}$$

Finally, the envelope expression for the initially inclined rotating body, $(\tan \sigma/2)_{env}$, is obtained simply from the product of equation (59) and the factor given in equation (52). The result is

$$\frac{(\tan \sigma/2)_{env}}{\tan \epsilon_p} = -\sqrt{\frac{\overline{\nu}}{K \tanh \frac{\pi \overline{\nu}}{2}}}\, \frac{G(\epsilon_p)}{\left(\frac{10}{9}\, e^{-1/3}\, \frac{1}{\beta R \sin \gamma_i}\right)^{1/4} \left(\frac{q}{q_{mh}}\right)^{1/4}} \tag{60}$$

Equation (60) reveals an interesting result. It will be noted that both K (eq. (47)) and ν (eq. (51)) are linear functions of ω. As $\tanh(\pi\overline{\nu}/2)$ is essentially unity for all values of $\overline{\nu}$ greater than about 1.5, equation (60) indicates that the effects on the envelope due separately to K^2 and ν cancel each other. On the one hand, increasing K^2 corresponds to increasing the turning rate of the liquid body, giving it a greater oblateness, and this in turn leads to a larger restoring moment which makes the envelope subside more rapidly. On the other hand, the inertial effect of the larger turning rate is to widen the envelope. These two opposing effects cancel. The result is that, regardless of the turning rate, all bodies formed by turning, having the same mass and the same initial inclination σ_i, will have identical angle-of-attack envelopes. Although this result has been obtained under the restriction of small turning rates, numerical solutions for larger rates indicate that it remains essentially true for all rates up to the limiting value ($K^2 = 1$) for which a figure of equilibrium exists.

Consider the application of this result to the southeast Australian tektites. Of all the round-form tektites that have been discovered in this region, none have been reported, to the authors' knowledge, to have any more than a small amount of oblateness; that is, in reference to figure 9, none apparently have primary figures corresponding to values of K^2 greater than perhaps 0.2. This means that if they had been formed by turning in the liquid state, their turning rates had to have been small. The analysis above leads one to expect that, as the tektites having small turning rates evidently were able to survive their passage through the atmosphere, tektites having forms

consistent with considerably larger rates should have been able to survive as well since their angle-of-attack envelopes should have been essentially the same. That such tektites apparently have not been found in southeast Australia therefore cannot be attributed to their having failed to survive their flight through the atmosphere, but must be charged to the mechanism by which the tektites were formed. The evidence is, then, that this mechanism was capable of imparting to the tektites only a very limited amount of angular momentum.

Effect of ablation.- The analysis of the preceding section should adequately describe the behavior of the round-form tektites over the initial portion of their entry into the atmosphere. As soon as ablation begins, however, the bodies undergo a marked change in geometry, and this must be taken into account in the analysis of their subsequent behavior. This may be done qualitatively within the framework of the present theory in view of the following: First, as in the preceding section, one need only study the case of planar motion and then multiply the result by the factor given in equation (52) to obtain the behavior of the rotating body. Second, in consideration of the planar motion, it may be said that the previous analysis will hold over the range of dynamic pressure from essentially zero to a value q_a at which ablation begins. Results of the ablation studies of reference 4 indicate that the ratio q_a/q_{mh} varies somewhat with entry conditions and tektite size. For entry conditions compatible with a lunar origin and for tektites the size of those found in southeast Australia, results from reference 4 indicate a value for the ratio of approximately 1/20. For convenience, let it be assumed that a peak in the oscillatory motion occurs in the vicinity of this point. The corresponding values of ϵ_p and $x(\epsilon_p)$ then may be determined from the preceding analysis and will serve as the initial conditions for the ensuing motion.

As ablation begins, the surface facing the stream will begin to recede, increasing its radius of curvature (cf. fig. 19, ref. 4). It is reasonable to assume that, though the angle of attack continually changes, the forward surface will continue to present an essentially spheroidal face to the stream. Hence, approximately, the aerodynamic force on the body will remain alined with the stream direction and pass through the center of curvature of the forward surface. This is illustrated on sketch (k). As the forward surface continues to recede, its center of curvature moves rearward. The center of gravity also moves rearward, but less rapidly than the center of curvature, so that the static margin ξ increases with time. The result is that the aerodynamic-restoring moment about the center of gravity retains the form

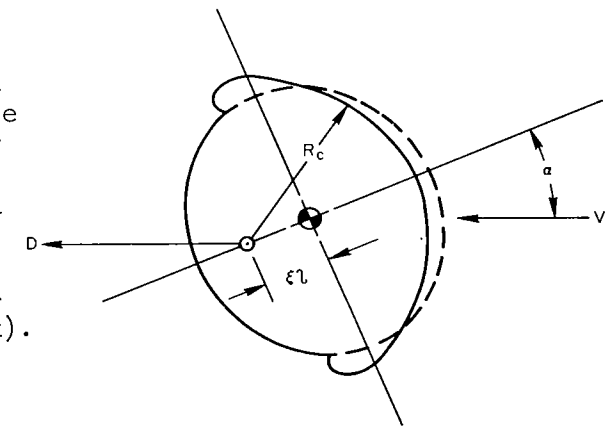

Sketch (k)

$$C_m = -C_D \xi \sin \alpha \qquad (61)$$

but now C_D and especially ξ are increasing functions of time. The equation of motion, equation (4), also retains the same form

$$\ddot{\alpha} - \frac{Al}{I} C_D \xi q(t) \sin \alpha = 0 \tag{62}$$

where now I also is a function of time. However, for the spheroidal body the changes in I and C_D are small enough to be neglected, or, in any case, I and C_D may be combined with ξ to give an "effective" value of that parameter. Finally, since both ξ and $q(t)$ increase with time, it may be assumed that, at least qualitatively, ξ increases as some power of q, that is,

$$\xi \approx \xi_a \left(\frac{q}{q_a}\right)^{\lambda} \tag{63}$$

where ξ_a and q_a are, respectively, the static margin and dynamic pressure at the beginning of ablation. On insertion of the exponential approximation for q (eq. (8)), the equation of motion becomes

$$\ddot{\alpha} - q_a \frac{Al}{I} C_D \xi_a e^{s(1+\lambda)t} \sin \alpha = 0 \tag{64}$$

which retains the form for the Painlevé transcendent. In effect, the increasing static margin causes the body to behave as though it were a nonablating body passing through an atmosphere with a larger density gradient than that actually existing.

With the form of the Painlevé equation retained, all of the results obtained previously for the planar oscillatory motion may be made applicable merely by a change in notation. Thus, let

$$\left.\begin{aligned} \bar{s} &= s(1 + \lambda) \\ \left(\frac{\bar{\kappa}\bar{s}}{2}\right)^2 &= -q_a \frac{Al}{I} C_D \xi_a \\ \bar{x} &= \bar{\kappa} e^{\bar{s}t/2} \end{aligned}\right\} \tag{65}$$

The asymptotic behavior of the envelope curve follows from equation (28)

$$\frac{(\tan \epsilon)_{env}}{\tan \epsilon_p} = \frac{C(\bar{\kappa}) G(\epsilon_p, \bar{\kappa})}{\sqrt{\bar{x}}} \tag{66}$$

It is useful to cast this result in terms of the dynamic pressure ratio q/q_{mh} where, as before, q_{mh} is the dynamic pressure at maximum heating. The result

is

$$\frac{(\tan \epsilon)_{env}}{\tan \epsilon_p} = \frac{C(\bar{\kappa})G(\epsilon_p,\bar{\kappa})}{\sqrt{\bar{\kappa}}\left(\frac{q_{mh}}{q_a}\right)^{(1+\lambda)/4}\left(\frac{q}{q_{mh}}\right)^{(1+\lambda)/4}} \tag{67}$$

The parameter $\bar{\kappa}$ may be related to the original coordinate x at the beginning of ablation through the expression

$$\bar{\kappa} = \frac{x(\epsilon_p)}{1 + \lambda} \tag{68}$$

Finally, the complete envelope curve for the planar motion, obtained from equations (59) and (67) is multiplied by the factor $\sqrt{(\pi\bar{\nu}/2)/[\tanh(\pi\bar{\nu}/2)]}$ to give the desired result $(\tan \sigma/2)_{env}$. Results obtained from the above analysis are shown on figure 10 for several values of the ablation parameter λ. The body has the mass of a sphere of 1-cm radius and a turning rate of 1 radian/sec. Entry conditions are those estimated in reference 4 to be compatible with a lunar origin:

$$V_i = 11.2 \text{ km/sec}$$

$$\beta = 0.1396 \text{ km}^{-1}$$

$$\gamma_i = 20^\circ$$

The main results are considered to be those shown on figure 10(a) for an initial inclination σ_i of 40° since if the initial inclination was truly arbitrary, the greatest number of tektites should have entered the atmosphere with inclinations near the mean between 0° and 90°. Figure 19 of reference 4 was used to establish a representative value of λ for tektites undergoing ablation under nonoscillatory conditions: Over the important initial period of ablation, during which time the radius of curvature of the front face increases very rapidly, λ was found to be of the order of 4 or 5. For the initially inclined rotating tektite, of course a smaller value must be expected, but it is seen on figure 10(a) that even a fraction of the full amount is sufficient to reduce

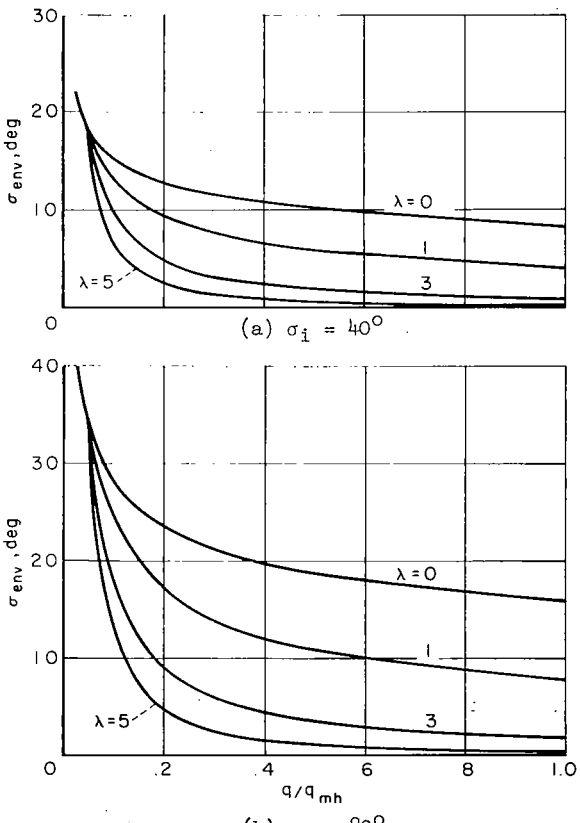

Figure 10.- Envelopes of resultant angles of attack of a rotating spheroidal tektite for a range of values of the ablation parameter λ; turning rate ω = 1 radian/sec.

σ to negligible proportions well before maximum heating. The results lead to the conclusion that entry conditions compatible with a lunar origin permit sufficient time for the greater part of the round-form Australian tektites to aline themselves with the stream well before maximum heating, in compliance with the physical evidence of their having undergone ablation under nonoscillatory conditions over the high heating portion of their trajectories. Shown on figure 10(b) are results for an initial inclination of 80°. It is noted that, if the same rate of ablation is allowed ($\lambda = 3$) as that which brought the body to negligible amplitudes in the case of a 40° initial inclination, here the body still retains a residual amplitude as maximum heating is approached, but of no more than a few degrees. Then in this case also, the final stage of ablation occurs with the body in an essentially fixed attitude with respect to the stream, so that the ring waves and coiled flanges characteristic of this stage should make their appearance on this body as well. On the other hand, since over the initial portion of the ablative process the inclination of the nose of the body was considerably greater than in the first case, the nose will have received considerably less heating than in the first case, and hence will have receded a lesser amount. The initial inclination must be considered to be arbitrary and therefore, for initially identical bodies, any amount of ablation is possible between the maximum, when the initial inclination is zero, and that for initial inclinations near 90°. It is believed that this explains how it can happen that initially identical tektites following identical trajectories may nevertheless show quite different depths of recession of their forward surface (cf. ref. 4).

Nonspheroidal shapes.- While the preceding analysis would appear to apply to the majority of the tektites found in southeast Australia (i.e., those of this region whose shapes are essentially spheroidal), it does not account for the remaining shapes, in particular the ellipsoids and "dumbbells." Figure 11 illustrates the three shapes, the original unablated forms being evident in the rear view. It is interesting to speculate on possible mechanisms that might account for the latter two forms. The fact that oblate spheroids, ellipsoids, and dumbbells make their appearance also in the study of rotating liquids when the contractive force is gravitation (ref. 12) suggests at first glance that the mechanism for the formation of tektites might have been of a similar nature. The investigation of this possibility was in fact what motivated the present research. In the gravitational case, the spheroids and ellipsoids form a progression of figures of equilibrium with increasing angular momentum, while the dumbbell or pear-shaped figure makes its appearance for values of angular momentum beyond that of the last stable ellipsoid (whether the pear-shaped figure is itself stable is a delicate and still controversial question). Unfortunately, the case for the existence of a parallel phenomenon for the tektites is untenable. When the contractive force is surface tension the figure of equilibrium must have cylindrical symmetry about the axis of rotation (ref. 14), which rules out both the ellipsoid and the dumbbell.

Two alternative phenomena may be envisaged: First, these bodies may have had angular momenta large enough to exceed the limiting value for which a stable figure exists. They would then have sought to rid themselves of part of their angular momentum, and this process could conceivably have led to the formation of elongated ellipsoids and dumbbells, these solidifying before they

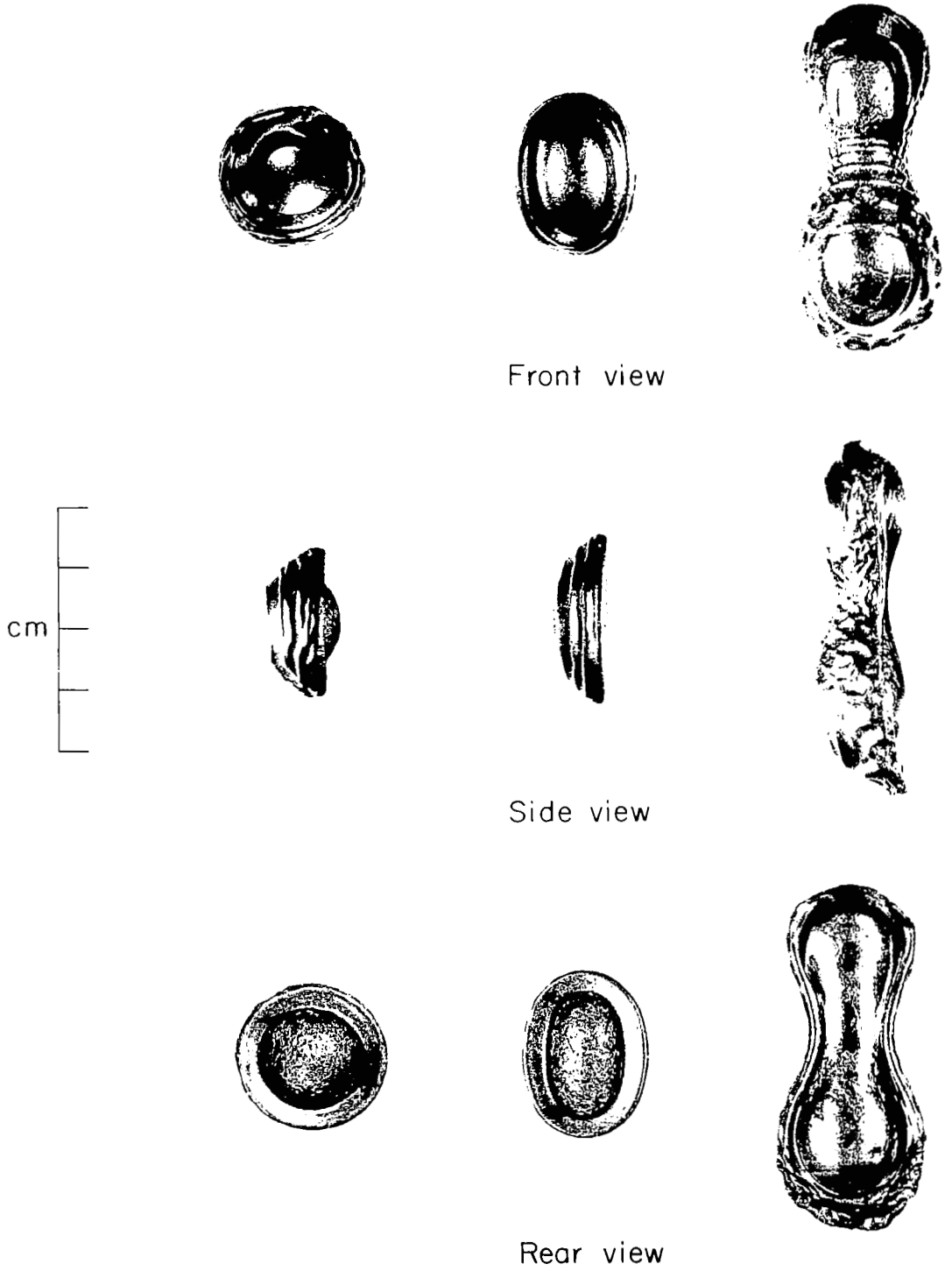

Figure 11.- Australian tektites having initially spheroidal, ellipsoidal, and dumbbell shapes. (Photograph of casts made from originals in British Museum.)

could break apart. Let us confine attention only to specimens of a common initial mass, and let the mass be that of a sphere of 1-cm radius, a characteristic shared by a large number of the specimens found in southeast Australia. Then according to the above hypothesis, the elongates must have had angular momenta in excess of approximately 170 dyne-cm-sec. On the other hand, spheroids of the same mass found in southeast Australia could have had angular momenta only of the order of 0-60 dyne-cm-sec on the presumption already noted that their values of K^2 were no larger than perhaps 0.2. Then there is a range of angular momenta from 60 to 170 dyne-cm-sec in which figures of equilibrium consistent with values in this range apparently have not been found in southeast Australia. As has been discussed, the dynamic behavior of these bodies should have been similar to that of surviving bodies having smaller values of angular momentum, and hence, there is no evident reason why they should have failed to appear. That is, if the elongates had been formed as the result of having an excess of angular momentum, then flattened spheroids should have been formed as well and should have been found in southeast Australia. This inconsistency leads one to doubt that the elongates could have had such large values of angular momentum and therefore to reject the idea that they could have been formed in the way envisaged above.

With rotation rejected as the mechanism by which the elongates acquired their form, a second alternative is the break-up of a slowly turning jet of liquid glass. As is well known (ref. 16), a jet of fluid is unstable and will exhibit ever-increasing harmonic undulations along its length. As shown in the upper section of sketch (*l*), a freed drop would tend to exhibit an ellipsoidal form, whereas, as in the lower section of the sketch, the drop would tend to the dumbbell form. Surface tension would then cause all forms to tend to the spheroidal. The appearance of all three forms on the surface of the Earth may be attributed to varying rates of solidification, some bodies having solidified before attaining their final forms.

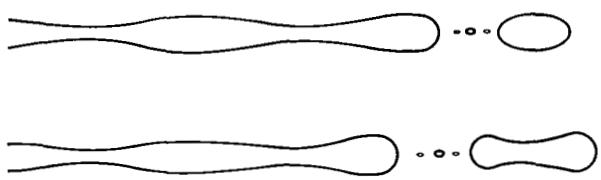

Sketch (*l*)

CONCLUDING REMARKS

The tumbling motion of aerodynamically stable bodies entering planetary atmospheres has been analyzed considering that the tumbling motion, its arrest, and the subsequent oscillatory motion are governed by the differential equation for the fifth Painlevé transcendent. A study of the asymptotic behavior of the transcendent enabled the functional relationship between the envelope of oscillatory motion and all the significant body and planetary properties to be demonstrated in a concise expression. Results were applied to the study of vehicles intended for use as planetary probes and it was shown how rapid estimates could be made of their probable amplitudes of oscillation in relation to aerodynamic heating and loads. The theory was also applied to a study of the motions of the southeast Australian tektites. It was concluded that with entry conditions

compatible with those for a lunar origin, a considerable range of initial turning rates and initial inclinations is admissible for the spheroidal tektites within which their amplitudes of oscillatory motions are reduced to negligible proportions before maximum heating. This complies with the evidence of their having undergone ablation at essentially fixed attitudes over the high heating portion of their trajectories. The admission of an initial inclination from the direction of flight of the axis about which the body turns leads to an explanation of how it can happen that initially identical tektites following identical trajectories may show significantly different depths of ablative recession of their forward surfaces. It is suggested that the mechanism by which the southeast Australian tektites acquired their forms was the break-up of a slowly turning jet of liquid glass.

Ames Research Center
National Aeronautics and Space Administration
Moffett Field, Calif., March 4, 1964

REFERENCES

1. Peterson, Victor L.: Motions of a Short 10° Blunted Cone Entering a Martian Atmosphere at Arbitrary Angles of Attack and Arbitrary Pitching Rates. NASA TN D-1326, 1962.

2. Tobak, Murray: Analytical Study of the Tumbling Motions of Vehicles Entering Planetary Atmospheres. NASA TN D-1549, 1962.

3. Peterson, Victor L., and Tobak, Murray: Theory of the Tumbling and Subsequent Large-Amplitude Oscillations of Vehicles Entering Planetary Atmospheres. Proc. of the Aerospace Forum, 1st Session, S.M.F. Fund Paper FF-34, 1963, pp. 74-81.

4. Chapman, Dean R., and Larson, Howard K.: On the Lunar Origin of Tektites. Jour. Geophys. Res., vol. 68, no. 14, July 1963, pp. 4305-58.

5. Sommer, Simon C., and Tobak, Murray: Study of the Oscillatory Motion of Manned Vehicles Entering the Earth's Atmosphere. NASA MEMO 3-2-59A, 1959.

6. Ince, E. L.: Ordinary Differential Equations. Dover Publications, New York, 1956.

7. Boutroux, P.: Recherches sur Les Transcendantes de M. Painlevé et L'Étude Asymptotique des Équations Différentielles du Second Ordre. École Normale Supérieure, Annales Scientifiques, ser. 3, vol. 30, 1913, pp. 256-375, and ser. 3, vol. 31, 1914, pp. 100-159.

8. Remmler, Karl L.: Tumbling Bodies Entering the Atmosphere. ARS Jour., vol. 32, no. 1, Jan. 1962, pp. 92-95.

9. Allen, H. Julian, and Eggers, A. J., Jr.: A Study of the Motion and Aerodynamic Heating of Ballistic Missiles Entering the Earth's Atmosphere at High Supersonic Speeds. NACA Rep. 1381, 1958.

10. Chapman, Dean R., Larson, Howard K., and Anderson, Lewis A.: Aerodynamic Evidence Pertaining to the Entry of Tektites into the Earth's Atmosphere. NASA TR R-134, 1962.

11. Chapman, Dean R.: On the Unity and Origin of the Australasian Tektites. Geochimica et Cosmochimica Acta, vol. 28, no. 6, June 1964, p. 841.

12. Lyttleton, Raymond A.: The Stability of Rotating Liquid Masses. Cambridge Univ. Press, England, 1953.

13. Charrueau, André: Étude d'une Masse Liquide de Révolution - Homogène, sans Pesanteur et à Tension Superficielle, Libre dans un Milieu à Pression Uniforme, Animée d'une Rotation Uniforme autour de son Axe de Révolution. École Normale Supérieure. Annales Scientifiques, vol. 44, 1927, pp. 129-176.

14. Appell, Paul: Traité de Mécanique Rationnelle. Vol. 4, part 1 - Figures d'Équilibre d'une Masse Liquide Homogène en Rotation. Gauthier-Villars (Paris) 1932, pp. 295-337.

15. Leon, Herman I.: Angle of Attack Convergence of a Spinning Missile Descending Through the Atmosphere. Jour. Aero/Space Sci., vol. 25, no. 8, Aug. 1958, pp. 480-484.

16. Rayleigh, John William Strutt, Baron: The Theory of Sound. Vol. 2, Macmillian and Co. (London) 1940, pp. 351-375.